STARS

University of Central Florida
STARS

Electronic Theses and Dissertations, 2004-2019

2010

Branched And Spiral Organic Nanotubes Based On The Self-assembly Of Bile Acids

Xuejun Zhang
University of Central Florida

 Part of the Materials Science and Engineering Commons
Find similar works at: https://stars.library.ucf.edu/etd
University of Central Florida Libraries http://library.ucf.edu

This Masters Thesis (Open Access) is brought to you for free and open access by STARS. It has been accepted for inclusion in Electronic Theses and Dissertations, 2004-2019 by an authorized administrator of STARS. For more information, please contact STARS@ucf.edu.

STARS Citation
Zhang, Xuejun, "Branched And Spiral Organic Nanotubes Based On The Self-assembly Of Bile Acids" (2010). *Electronic Theses and Dissertations, 2004-2019*. 1698.
https://stars.library.ucf.edu/etd/1698

www.manaraa.com

BRANCHED AND SPIRAL ORGANIC NANOTUBES BASED ON THE SELF-ASSEMBLY OF BILE ACIDS

by

XUEJUN ZHANG
B.S, Chemical Engineering, 1999, Qingdao University of Science and Technology
M.S, Materials Physical Chemistry, 2005, Nankai University
PhD in Physical Chemistry, 2009, Nankai University

A thesis submitted in partial fulfillment of the requirements
for the degree of Master of Materials Science and Engineering
in the Department of Mechanical, Materials and Aerospace Engineering
in the College of Engineering and Computer Science
at the University of Central Florida
Orlando, Florida

Fall Term
2010

www.manaraa.com

© 2010 Xuejun Zhang

www.manaraa.com

ABSTRACT

The self-assembly of chiral amphiphilic molecules in aqueous solutions is of particular interest because the chirality of individual molecules is often expressed in their supermolecular structures. Self-assembled tubes made of chiral amphiphilic molecules represent useful supramolecular architectures which hold promise as controlled release vehicles for drug delivery, encapsulates for functional molecules, and nanoreactors for chemical reactions.

Lithocholic acid (LCA) is a secondary bile acid with the concentration being identical to that of cholesterol in the hepatic bile and gallbladder. It has a rigid, nearly planar hydrophobic steroid nucleus, with four hydrogen atoms and one hydroxyl group directed toward the concave side, and the convex side with three methyl groups. The ionic head with a carboxyl group is linked to the steroid nucleus through a short alkyl chain.

In this thesis work, I study the self-assembly behavior of LCA at the liquid-solid interface, in confined spaces, and bulk solution. We find that the initially formed LCA vesicles further assemble into fractal tubes on glass slides by diffusion-limited aggregation and pronglike tubes by the capillary flow generated in an evaporating vesicle solution confined by two parallel glass slides. While in bulk solution, the LCA vesicles linearly aggregate and fuse into spiral tubes at pH 12.0. The spiral tubes can transition into a straight shape as the pH of solution is reduced to 7.4. The shape transition of the tubes is reversible as the pH of solution is adjusted back to 12.0. The pH-switchable shape transition suggests that the self-assembled LCA tubes can act as a supramolecular chemical spring.

Finally, the LCA tubes are endowed with optical functionality by embedding cadmium sulfide nanopaticles (CdS) in the tube walls by the co-assembling synthesis of cadmium sulfide

www.manaraa.com

(CdS) nanoparticles with lithocholic acid (LCA) molecules. The fluorescent composite tubes can undergo pH switchable spiral/straight, which are a promising system for a variety of materials and biological applications.

www.manaraa.com

Dedicated to

My parents, husband and sisters

www.manaraa.com

ACKNOWLEDGMENTS

I would like to take this opportunity to express my sincere gratitude towards my advisor Dr. Jiyu Fang, for his help and support throughout my study and research. I appreciate his constant guidance, encouragement, and valuable discussion. I would also like to thank Profs. Linan An, and Andre J. Gesquiere for serving on my dissertation committee and their suggestions. I also want to thank fellow graduates Karan Tamhane, Wenlong Liang; and my friends, Jianhua Zou.

Most importantly, words cannot truly express my deepest gratitude towards my parents, husband, sisters and parents in law who always gave me their love and spiritual support.

www.manaraa.com

TABLE OF CONTENTS

LIST OF FIGURES x

CHAPTER 1: INTRODUCTION 1

1.1 Self-assembly of biological molecules 1

1.2 Self-assembly of amphiphilic biomolecules 1

1.2.1 Fatty acids 2

1.2.2 Lipids 2

1.2.3 Steroids 4

1.3 Bile acids 4

1.3.1 Chemical structures of bile acids 5

1.3.2 Micelle formation in aqueous solutions 7

1.3.3 Supramolecular chirality and chiral chain in molecular assemblies 8

1.3.4 Supramolecular association leading to hydrogelation 10

1.3.5 Bile Acids in Pharmacological and Supramolecular Applications 12

1.4 Conclusions and prospects 13

1.5 References 13

CHAPTER 2: ASSEMBLY OF VESICLES INTO FRACTAL AND PRONG PATTERNS ON SUBSTRATES 19

2.1 Introduction 19

2.2 Experimental and methods 20

2.2.1 Synthesis of LCA vesicless 20

2.3 Results and discussion 21

2.3.1 Structure change vesicles 21

2.3.2 Fractal growth of vesicles 23

www.manaraa.com

2.3.3 Surface tention induced vesicles arrangement 26
2.4 Conclusions 29
2.5 References 30
CHAPTER 3: SELF-ASSEMBLY OF pH-SWITCHABLE SPIRAL TUBES: SUPRAMOLECULAR CHEMICAL SPRINGS 34
3.1 Introduction 34
3.2 Experimental and methods 35
3.2.1 Synthesis of LCA tubes 35
3.2.2 Characterization 36
3.3 Results and discussion 36
3.3.1 Growth of LCA tube in solution 36
3.3.2 Conformation change triggered by pH value 40
3.2.3 Mechanic property of LCA tube 43
3.4 Conclusions 44
3.5 References 45
CHPATER 4: FLUORESCENT COMPOSITE TUBES WITH PH-CONTROLLED SHAPES 50
4.1 Introduction 50
4.2 Experimental sections 52
4.2.1 Chemicals and materials 52
4.2.2 Synthesis of LCA/CdS composite tubes 52
4.2.3 Characterization of LCA/CdS composite tubes 53
4.3 Results and discussion 54
4.3.1 Structure of LCA/CdS tubes 54
4.3.2 Optical properties of LCA/CdS compsite tubes 58
4.3.3 Conformation changes of LCA/CdS composite 61
4.4 Conclusions 64

www.manaraa.com

4.5 References 65

www.manaraa.com

LIST OF FIGURES

Figure 1.1 Cross sections of spherical or discoid phospholipid aggregates: (A) liposomes, (B) supported bilayers on microspheres, (C) monolayers on alkylated microspheres, (D) nanodisks, (E) immobilized artificial membranes, and (F) bicelles. The schematic structures are not drawn to proportion. As introduced by Chemical Review. 3

Figure 1.2 Bile acids chemical structure and their facial amphiphilic structure: hydrophobic (lipid soluble) and hydrophilic (polar) faces. 6

Figure 1.3 Cartoon representations of bile salt micelles (primary and secondary aggregation model) as introduced by Small. 8

Figure 1.4 Schematic description of hierarchical structure of bile acids from primary structure: molecular structure, secondary structure: chiral helical tape to tertiary structure, bundle structure of the chiral helical tapes, as introduced by Molecules. 10

Figure 1.5 SEM of an aqueous gel of a cationic bile acid derivative, as introduced by Chem. Soc. Rev. 11

Figure 1.6 Photographs of gels from the tripodal cholamide (a) colorless gel and luminescent gel (handheld long wave UV lamp); (b) cryo-TEM image of the gel, as introduced by Org. Biomol. Chem. 12

Figure 2.1 (a) Optical microscopy image of self-assembled LCA vesicles in aqueous solution at pH of 12.0. (b) FT-IR spectrum of LCA vesicles dried on an ATR crystal. 22

Figure 2.2 Optical microscopy images of a fractal assemble of LCA vesicles on glass slides by diffusion-limited aggregation. These glass slides were immersed in vesicle solution for 15 mins (a), 120 mins (b) and 24 hours. These images were taken immediately after glass slides were withdrawn from vesicle solution. 23

Figure 2.3 Optical (a) and polarizing (b) microscopy images of a fractal pattern of LCA vesicles on a glass slide. The enlarged image of the branches of the fractal pattern was inset in Figure 3a. (c) Box-counting calculation of the fractal pattern. The slope of the linear fitting of the log-log plot of n(ε) versus ε is -1.746. 24

Figure 2.4 Optical microscopy images of the growth of a micron sized channel from the receding contact line of the vesicle solution confined by two parallel glass slides. Time interval of these images was 2 seconds. The vesicles pulled into the channel by capillary flow. 26

Figure 2.5 (a) Optical microscopy image of two parallel channels with a clump made of vesicle aggregates at their ends. The clump acts a pinning point at which each channel starts. (b) Optical

www.manaraa.com

microscopy image of two parallel channels that are forced together by the nonuniform motion of the receding contact line to form a prong like pattern. 27

Figure 2.6 Optical microscopy images of parallel arrays (a) and prong like patterns (b and c) of LCA vesicles assembled on glass substrates. 28

Figure 2.7 Optical microscopy images of fractal (a) and prong like patterns (b) of LCA tubes formed by fusion of linearly aggregated LCA vesicles in small fractals and channels on glass substrates. 29

Figure 3.1 (a) Chemical structure of lithocholic acid. Optical microscopy images of self-assembled structures of LCA molecules in alkaline solution (pH 12.0) at room temperature after 2 hours (b), 6 hours (c), and 3 days (d). 37

Figure 3.2. (a-c) Optical microscopy images of the deposition process of a 3D left-handed spiral tube on a glass substrate during water evaporation in air. (d) Polarizing microscopy image of a 3D spiral tube in aqueous solution. (e) X-ray diffraction of spiral tubes dried on a glass substrate. The direction of the polarizer and analyzer is indicated by while arrows in (d). 38

Figure 3.3 (a-b) Optical microscopy images of disassembly of large tubes in aqueous solutions at pH 12.0 after a month. The separated small tubes coil into spiral shapes. 40

Figure 3.4 (a-b) Optical microscopy images of the shape transition of coiled tubes in aqueous solutions when the pH was reduced from 12.0 to 7.4. The images were taken after adding HCl for 1 min (a) and 3 min (b). (c) TEM image of a straight tube dried on a carbon-coated grid. The TEM image of the end of a tube is inset in (c). (d) Electron diffraction pattern of tube walls. The TEM measurements were carried at room temperature. 41

Figure 3.5. FT-IR spectra of spiral (a) and straight (b) tubes dried on an ATR crystal. 42

Figure 3.6 Optical microscopy images of coiled (a) and straight (b) tubes adsorbed on glass substrates after 40 scans under a loading force of 29.93 nN in aqueous solutions at pH 12.0 and pH 7.4, respectively. These images were taken with the optical microscope built into the AFM.44

Figure 4.1 (a) Optical microscopy image of composite LCA/CdS tubes in aqueous solution at pH 13.0. (b) Low resolution TEM image of a LCA/CdS tubes dried on a carbon-coated grid. (c-d) high resolution TEM images of individual CdS nanoparticles embedded in LCA membrane walls. 55

Figure 4.2 (a) FT-IR spectra of pure LCA tubes and composite LCA/CdS tubes dried on an ATR crystal. (b) UV-vis spectrum of composite LCA/CdS tubes in aqueous solution. Both FT-IR and UV-vis spectra were taken at room temperature. 57

Figure 4.3 (a) Fluorescence confocal image of a composite LCA/CdS tubes in aqueous solution at pH 9.5. (b) Fluorescence spectrum taken from a simple point at the composite LCA/CdS tube shown in (a). 58

www.manaraa.com

Figure 4.4 (a) Fluorescence confocal image of a composite LCA/CdS vesicle in aqueous solution at pH 13.0. (b) Low-resolution TEM image of a collapsed LCA/CdS vesicle on a carbon-coated grid. (c) EDX spectrum of the collapsed LCA/CdS vesicle shown in (b). (d) high-resolution TEM images of individual CdS nanoparticles embedded in the collapsed LCA/CdS vesicle shown in (b). 60

Figure 4.5 (a) Fluorescence confocal image of linearly aggregated composite LCA/CdS vesicles in aqueous solution at pH 13.0. (b) Fluorescence confocal image of composite LCA/CdS tubes in aqueous solution at pH 13.0. (c) Enlarged Fluorescence confocal image of the selected are in (a). (d) Optical microscopy image of helical composite LCA/CdS tubes in aqueous solution at pH 13.0..... 61

Figure 4.6 Optical microscopy (a) and fluorescence confocal (b) images of composite LCA/CdS plates in aqueous solution at pH 7.0. Optical microscopy (c) and fluorescence confocal (d) images of composite sheaves in aqueous solution at pH 5.0. 63

www.manaraa.com

CHAPTER 1: INTRODUCTION

1.1 Self-assembly of biological molecules

Self-assembly of biological molecules provides striking illustrations in building functional architectures in nature, including the self-assembly of lipids into cell membranes, the formation of double helical DNA through hydrogen bonding of individual strands, and the assembly of peptides or proteins to form quaternary structures. In the last decade, self-assembled biological systems have been employed as a model to develop the synthetic architectural motifs. Considerable advances have been made in the use of biomolecules, such as lipids, amino acids, nucleotides, peptides, and DNA as building blocks to produce potential useful materials[1]. For example, self-assembled ribbons, fibers, and tubes of peptides and proteins have recently emerged as unique templates to synthesize inorganic nanostructures for nanotechnology applications[2]. The self-assembly of biological molecules also allows the construction of other useful structures such as micelles[3], membranes[4], vesicles[5], liquid crystals[6] and gels[7]. In general, biological molecules provide us a range of well-studied structural and functional building blocks to build up functional architectures.

1.2 Self-assembly of amphiphilic biomolecules

Amphiphilic molecules with distinct hydrophobic and hydrophilic segments are versatile building blocks. It has been shown that amphiphilic molecules can self-assemble into diverse aggregate mophologies[8]. The self-assembly is mediated by non-covalent interactions, such as hydrogen bonding, metal coordination, hydrophobic forces, van der Waals forces, π-π

www.manaraa.com

interactions and electrostatic effects.[9] Although these bonds are relatively insignificant in isolation, the cluster of them can provide strong adhesions, which stabilize the self-assembled aggregates.[10-12] Here, I am discussing the self-assembly behavior of fatty acids, lipids, steroids, and bile acids.

1.2.1 Fatty acids

Fatty acids are an amphiphilic molecule with a hydrophobic hydrocarbon tail and a hydrophilic carboxyl head. They are derived either from endogenous metabolism or by nutritional sources and play significant roles in the biological signaling processes of cell membranes and the production of biologically active compounds. Recently, the structure of dietary fatty acids has become an important issue in human health because the ingestion of saturated fats (containing triglycerides composed of saturated fatty acids) is considered harmful, while unsaturated fats are viewed as beneficial.[13] Fatty acids are also unique building blocks in the synthesis of supramolecular materials. For instance, oleic acid can form vesicular membranes under the defined conditions of pH, ionic composition, and concentration. They have used for the growth and encapsulation of functional polymerase enzymes.

1.2.2 Lipids

Lipids are an amphiphilic molecule with two hydrophobic tails and a hydrophilic head. They are a major component of cell membranes[14]. Dietary lipids also play an important role as sources of essential fatty acids, needed for normal growth and survival[18].

www.manaraa.com

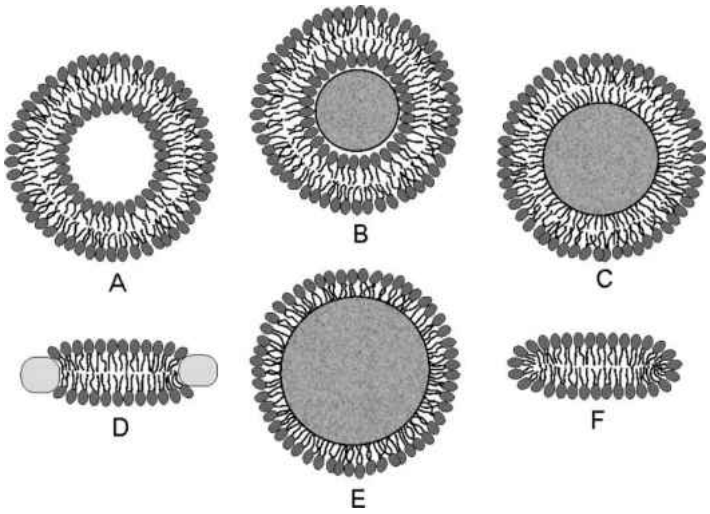

Figure 1.1 Cross sections of spherical or discoid phospholipid aggregates: (A) liposomes, (B) supported bilayers on microspheres, (C) monolayers on alkylated microspheres, (D) nanodisks, (E) immobilized artificial membranes, and (F) bicelles. The schematic structures are not drawn to proportion. As introduced by Chemical Review.

Depending on experimental conditions, lipids can self-assemble into aggregates with different morphologies such as spherical, discoid, or oblate ellipsoid shapes (see Figure 1.1)[19]. Liposomes are spherical corpuscles consisting of the aqueous central phase surrounded by one (Figure 1.1A) or more lipid bilayers, which are separated by a thin layer of water. The immobilized and supported liposomes (Figure 1.1B) have a long history of being used as surrogate systems for cell membranes. Unlike micelles, liposomes have both aqueous interiors and exteriors. In most cases, unilamellar vesicles are preferred to multilamellar liposomes. Based on their sizes, liposomes are classified into three categories: the minimum-size unilamellar vesicles (diameters of 15-30 nm), large unilamellar vesicles (up to several hundred nanometers), and giant unilamellar vesicles (on the order of micrometers). Chiral lipids have shown the ability of self-assembling into hollow cylindrical tubular structures with open ends.[15, 16] The

www.manaraa.com

self-assembled lipid tubules are potential useful supramolecular building blocks in the design of materials[12, 17].

1.2.3 Steroids

Steroids are widely distributed in animals, where they are associated with a number of physiological processes. Examples of steroids include cholesterol, the sex hormones estradiol and testosterone, and dexamethasone. The general structure of steroids consists of two six-membered rings sharing one side in common, a third six-membered ring off the top corner of the right ring, and a five-membered ring attached to the right side of that. Substituent groups at different sites on the tetracyclic skeleton have fixed axial or equatorial orientations because of the rigid structure of the trans-fused rings. Unlike more traditional amphiphilic molecules, which typically have a hydrophilic head group bonded to a linear, flexible, hydrocarbon tail, Steroids have with a hydrophilic α face and a hydrophobic β face. This unusual facial amphiphilic nature makes them unique building blocks in assembling supramolecular materials.

1.3 Bile acids

Bile acids are the most important group in steroids. They are versatile building blocks for the design of frameworks capable of ionic and molecular recognition. Bile acid-based compounds have found use in the transport of ions and molecules across phospholipid bilayers. The inclusion complexes and combinatorial libraries of bile acids are useful in the investigations of selective interactions between a host and a guest. They have been used as a chiral template in the asymmetric syntheses and act as an organogelator to form hydrogels, offering potential applications in medicine, pharmacology, cosmetics, material science, and environmental

www.manaraa.com

clean-up. A vast amount of interesting medical applications, such as potential cancer and HIV therapeutic agents based on bile acids have been reported[20, 21].

1.3.1 Chemical structures of bile acids

Bile acids and bile salts are natural biosufactants, which act as a solubilizer and an emulsifier for cholexterol, lipids, and proteins in the intestine[22 23]. The most abundant mammalian bile acid is the hydroxyl derivative of cholanoic acid (5b-cholan-24-oic acid), and in humans these consist mainly of cholic acid and chenodeoxycholic acid, in the forms of the irglycine and taurine conjugates (-$NHCH_2COO$- and -$NHCH_2CH_2SO_3$- at C-24). [24 25, 26] Cholic and chenodeoxycholic (and its 7-hydroxyepimerursodeoxycholic acids) have important pharmaceutical applications related to their ability to dissolve cholesterol gall stones and for the treatment of bile acid deficiency and cholestaticliver diseases. [27-31] The bile acid group also includes deoxycholic acid and lithocholic acid, commonly known as secondary bile acids. They are produced from cholic and chenodeoxycholic acids by the dehydroxylation by the intestinal bacteria.

As we mentioned before, bile salts constitute a large family of molecules, which are composed of two connecting units, a rigid steroid nucleus and a short aliphatic side chain. The different numbers of hydroxyl groups are presented the both sides of the rigid steroid nucleus (Figure 1.2). The steroid nucleus of bile acids contains the saturated tetra-cyclic hydrocarbon rings (three six-member rings (A, B and C) and a five-member ring (D)). In higher vertebrates, the bile acid nucleus is curved (beaked) because the A and the B rings are in a cis-fused configuration. The bile acid nucleus in lower vertebrates, known as allobile acids, is flat because of an A/B trans-fusion (5a-stereochemistry). The structure of the side chains determines the class of the bile acid (four major types of bile acids or bile alcohols). They occur in the less evolved

www.manaraa.com

forms of life. In higher vertebrates, C24 bile acids constitute a major part of the bile. They are conjugated to glycine or taurine to yield the conjugated form of bile acids. Bile acids are facial amphiphilic molecules with hydrophobic and hydrophilic faces.

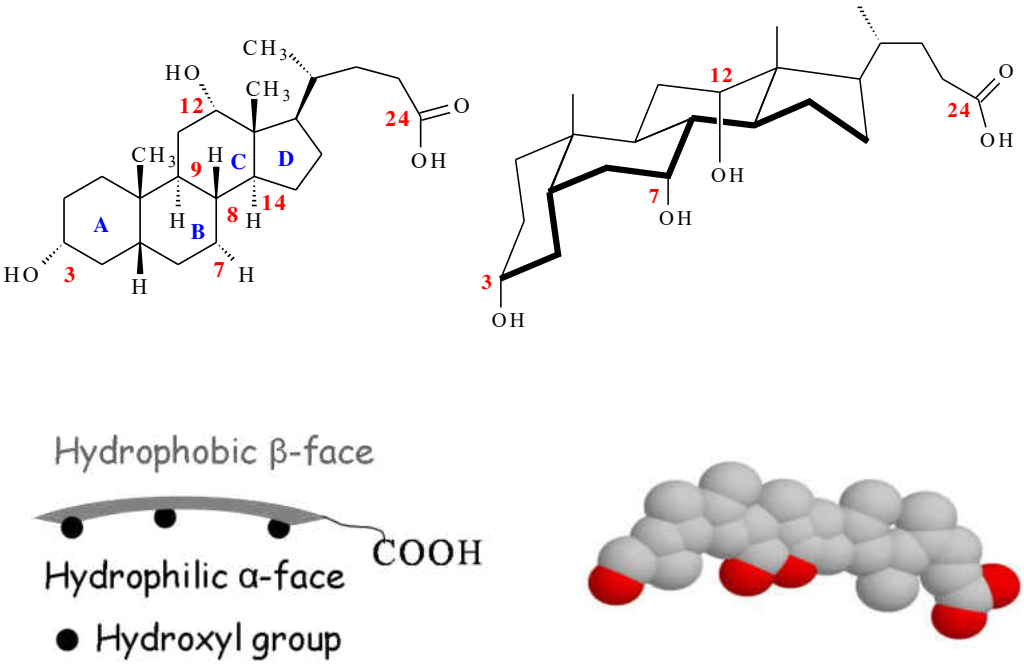

Figure 1.2 Bile acids chemical structure and their facial amphiphilic structure: hydrophobic (lipid soluble) and hydrophilic (polar) faces.

Bile acids can also be transformed into many derivatives by various chemical methods. For example, their carboxyl group side-chains can be changed to amide, ester, and hydroxyl groups, and the hydrogen ion of which can be substituted by other basic ions such as Na^+. Such chemical modification brought about a great amount of new host compounds with characteristic inclusion abilities.

www.manaraa.com

1.3.2 Micelle formation in aqueous solutions

In aqueous environments, bile salts aggregate to form micelles[19]. These micelles, under physiological conditions, are transformed into mixed-micelles with lecithin and glycerides, which are responsible for fat/cholesterol solubilization in the small intestine[32]. Bile acids are lipid-carriers and are able to solubilize many lipids by forming mixed micelles with fatty acids, cholesterol and mono-glycerides. These micelles are responsible for the solubilization and absorption of fat-soluble vitamins such as vitamin E.[33] The physical chemistry of micellization of bile salts has been, and still is, an active area of research. A variety of state-of-the-art techniques have been employed in order to gain more insights into the structure/size/shape of bile-salt micelles. This section will deal with both concepts and techniques (classical and advanced) used to understand structure and dynamics of bile-salt micelles.

Unlike conventional surfactant molecules, bile salts possess a rigid steroid backbone having polar hydroxyl groups on the concave α-face and methyl groups on the convex β-face (Figure 1.1). This arrangement creates a unique facial amphiphilicity for this class of molecules, enabling them to aggregate in aqueous media in a manner different from conventional detergents. Aggregation of bile salts in aqueous solution is largely driven by the hydrophobic association of apolar β-faces of steroid backbones, while further aggregation occurs through hydrogen bonding interactions (Figure 1.6). Micelles can solubilize guest molecules in their core, above the critical micellar concentrations (CMC) of the detergents, and this phenomenon (dye solubilization) has routinely been used to determine CMC values. As we know that bile acid can form dendrons. With these dendrimers, the “micellar structures” are maintained at all concentration ranges and thus the guest solubilization increaseds linearly with concentration. Kobuke et al.[34] have used an

www.manaraa.com

amphiphilic bile acid unit for the construction of a dendritic bile acid oligomers with a remarkable ability to act as both normal and inverse micelles owing to the facially amphiphilic nature of the bile acid backbone. Because of the free hydroxyl groups in the periphery, these dendrons are believed to adopt different conformations in solvents of different polarities (adaptive dendrons), which enable them to mimic both unimolecular normal and inverse micelles.

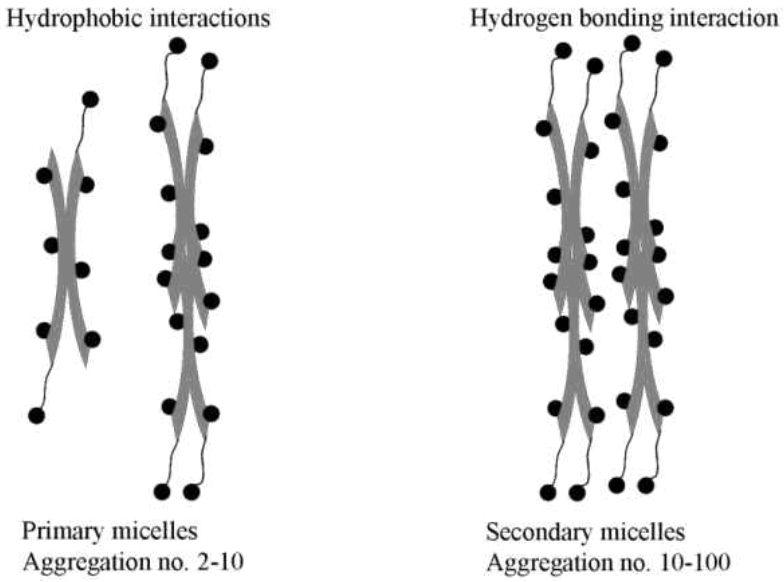

Figure 1.3 Cartoon representations of bile salt micelles (primary and secondary aggregation model) as introduced by Small.

1.3.3 Supramolecular chirality and chiral chain in molecular assemblies

It is confirmative that prediction of crystal structures still remains a challenging subject for many chemists. It has been controversial that how or if the chiral molecular express their chirality in their assemblies. Mikiji Miyata group has been using computational approuches and modeling simulation of different types of bile acids and their derivatives to interpret that

www.manaraa.com

biomolecules which have a common asymmetric structure with three different directions tend to form characteristic inclusion crystals with hierarchical structure.[35] Such hierarchical structure enables us to explain a role of the side-chains with different hydrogen bonding groups and length.[36-39] This concept induced the subsequent idea that the steroidal molecules must make their hierarchical assemblies with chirality in the crystalline state. In other words, the assemblies may exhibit supramolecular chirality in the crystalline state. Namely, each hierachical assembly of the steroidal molecules must have its own three-dimensinonal structures with chirality, starting from the original molecular chirality, as shown in Fiure 1.5. The chiral chains may dominate chirality of the subsequent assemblies, such as helices, bundles, and host-guest complexes. However, it is difficult to interpret this factor that the steroidal molecules form diverse assemblies, such as monolayers, bilayers, helicaltubes, and so on.

However, even in helices structure, current explanations of the self-assembly of helices are based on theories of multilamellar liquid crystal bilayers or hexatic phases encounter questioning. These theories assume that helices correspond to two different molecular packings within the bilayer and further that molecular chirality is the driving force behind helix formation. The results of Zastavker and Thomas *et al.* [40] suggest that chirality is not the only factor in helix formation.[40] Their experimental finding suggests that if both a nonplanar sterol nucleus and a 3α-hydroxy group (i.e., a sterol possessing a planar sterol nucleus and a 3α-hydroxy group) are present, then helices will not form. In addition, the sterol side chain does not seem to affect the formation of helices. If indeed helical ribbons are crystalline in nature, the crystal structures of the sterols for which helices are formed should be similar. Furthermore, any change in the sterol structure that affects crystal formation should affect helix formation.

www.manaraa.com

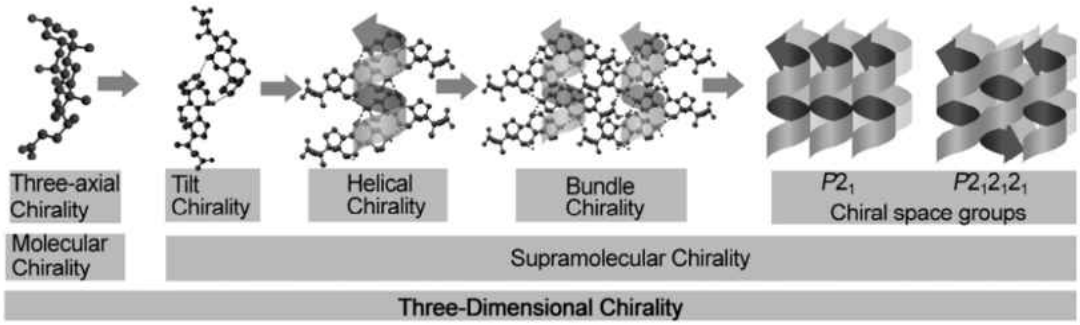

Figure 1.4 Schematic description of hierarchical structure of bile acids from primary structure: molecular structure, secondary structure: chiral helical tape to tertiary structure, bundle structure of the chiral helical tapes, as introduced by Molecules.

1.3.4 Supramolecular association leading to hydrogelation

Supramolecular gelators or hydrogels find applications in a wide variety of areas such as drug-delivery systems, tissue engineering and semi-wet biomaterials for protein microarrays, sensor, medicine, pharmacology, cosmetics, hardeners of spilled toxic solvents and environmental clean-up[7, 41, 42]. The intrinsic property of bile acids/salts to self-assemble hierarchical structures with respect to cooperative interactions composed of multiple non-covalent bonding groups makes them amenable to form gels in different solvents. This unusual behavior of bile acids was known for a long time. Sodium cholate, sodium deoxycholate and sodium lithocholate were shown to form gels in water. Gels are materials with intriguing features owing to the coexistence of solid (the networked fibrous structure) and liquid phases (entrapped solvent molecules). Figure 1.6 shows a typical SEM image of such a gel matrix formed by the self-assembly of an aqueous gelator[41]. However, some of these interesting observations remained unnoticed by several researchers in this area. For instance, X-ray diffraction studies performed by Rich and Blow on the deoxycholate gel revealed that the (supra)

www.manaraa.com

molecular complex formed a helical structure with 36 Å diameter. The complex formation (gelation) was favoured at lower pH and higher ionic strength.

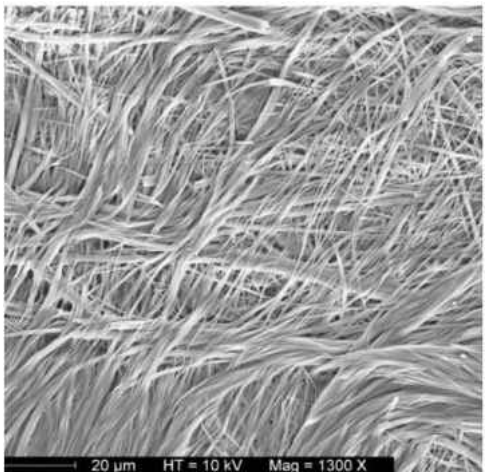

Figure 1.5 SEM of an aqueous gel of a cationic bile acid derivative, as introduced by Chem. Soc. Rev.

As many supramolecular hydogels are derived from naturally occurring molecules, bile acids and their derivatives are likely to be biocompatible and may therefore be explored for similar application. Nonappa and Uday Maitra group have fabricated efficient gelation of queous fluids by a cholic acid trimer (tripodal cholamide).[19, 43] The gel showed the presence of nanofibres, amazingly, it turned highly fluorescent dropping a plarity-sensitive fluorescent dye ANS and a thermalchromic gel can be developed after it is doped with bromophenol (Figure 1.7). These gels appear to be excellent soft materials for futuristic applications because of their remarkable water-holding ability and the solubilzation of flat, nonpolar molecules.

www.manaraa.com

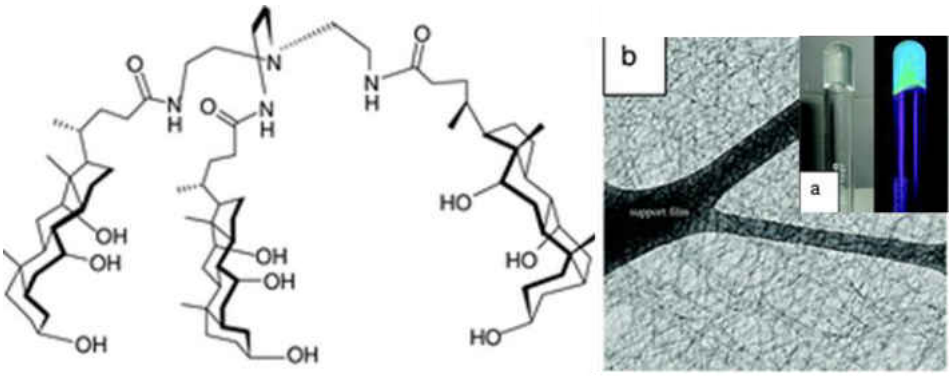

Figure 1.6 Photographs of gels from the tripodal cholamide (a) colorless gel and luminescent gel (handheld long wave UV lamp); (b) cryo-TEM image of the gel, as introduced by Org. Biomol. Chem.

1.3.5 Bile Acids in Pharmacological and Supramolecular Applications

Bile acids and their derivatives are also important compounds from the pharmacological point of view. Cholic acid, chenodeoxycholic acid, and ursodeoxycholic acid (3α,7β-dihydroxy-5β-cholan-24-oic acid) and their conjugates have been used in the treatment of bile acid deficiency and live diseases as well as in dissolution of cholesterol gallstones[44]. Nor- and homo-bile acid derivatives have potential to act as carriers of liver-specific drugs, absorption enhancers, and as cholesterol level lowering agents. In the body, bile acids combine with glycine and tourine forming amides, which are hydrolysed by intestinal bacteria in the metabolic pathway. Therefore, it is expected that analogous polymeric bile acid derivatives would also have a tendency of being biodegradable, or exhibit other biological activity. Antiviral properties of bile acids and their sulfate derivatives[45] as well as antifungal properties of some bile acid esters[46] have been added to some medicaments in order to improve their absorption. Bile acid polyamine conjugates are potential agents in gene therapy because of the Coulombic attraction between the polyamine moieties and the polyphosphate backbone of deoxyribonucleic acid.

www.manaraa.com

Polymeric bile acids and insulin conjugates can be used for the production of a medicament for diabetes mellitus. Bile acid derivatives conjugated with metal ion chelated complexes have been used successfully as contrast agents in magnetic resonance imaging (MRI). For example, they have been used in MRI assessment of micro vascular hyperpermeability in a rat breast tumor as well as an anti-VEGF (vascular endothelial grown factor) agent and as blood pool agents for NMR diagnostics.

1.4 Conclusions and prospects

Bile acids are versatile building blocks for the design of architectures for new materials and frameworks capable of ionic and molecular recognition. The facial amphiphilicity and rigid steroid backbone of bile acids seem to be most important in the expression of their chemical/supramolecular/biological/physio-logical properties. Additionally, the diverse and unique properties of bile acids pertaining to both chemistry and biology arise from their structural uniqueness. They have been used as a chiral template in the asymmetric syntheses and a gelator in the formation of hydrogels, which could have potential for drug delivery. Bile acid-based systems are also important for detailed understanding of the functioning of natural systems and for the development of new chemical and pharmacological applications.

1.5 References

1. Ikkala, O.; ten Brinke, G., Functional materials based on self-assembly of polymeric supramolecules. *Science* **2002,** 295, (5564), 2407.

2. Aggeli, A.; Nyrkova, I. A.; Bell, M.; Harding, R.; Carrick, L.; McLeish, T. C. B.; Semenov, A. N.; Boden, N., Hierarchical self-assembly of chiral rod-like molecules as a model

www.manaraa.com

for peptide -sheet tapes, ribbons, fibrils, and fibers. *Proceedings of the National Academy of Sciences of the United States of America* **2001,** 98, (21), 11857.

3. Zhang, S., Fabrication of novel biomaterials through molecular self-assembly. *Nature biotechnology* **2003,** 21, (10), 1171-1178.

4. Salditt, T.; Schubert, U. S., Layer-by-layer self-assembly of supramolecular and biomolecular films. *Reviews in Molecular Biotechnology* **2002,** 90, (1), 55-70.

5. Vauthey, S.; Santoso, S.; Gong, H.; Watson, N.; Zhang, S., Molecular self-assembly of surfactant-like peptides to form nanotubes and nanovesicles. *Proceedings of the National Academy of Sciences of the United States of America* **2002,** 99, (8), 5355.

6. Huie, J. C., Guided molecular self-assembly: a review of recent efforts. *Smart Materials and Structures* **2003,** 12, 264.

7. Pal, A.; Basit, H.; Sen, S.; Aswal, V. K.; Bhattacharya, S., Structure and properties of two component hydrogels comprising lithocholic acid and organic amines. *Journal of Materials Chemistry* **2009,** 19, (25), 4325-4334.

8. Shimizu, T.; Masuda, M.; Minamikawa, H., Supramolecular nanotube architectures based on amphiphilic molecules. *Chem. Rev* **2005,** 105, (4), 1401-1444.

9. Lindsey, J. S., Self-assembly in synthetic routes to molecular devices. Biological principles and chemical perspectives: a review. *New J. Chem* **1991,** 15, 153?80.

10. Bromley, E. H. C.; Channon, K.; Moutevelis, E.; Woolfson, D. N., Peptide and protein building blocks for synthetic biology: from programming biomolecules to self-organized biomolecular systems. *ACS Chemical Biology* **2008,** 3, (1), 38-50.

www.manaraa.com

11. Jung, J. H.; Shimizu, T.; Shinkai, S., Self-assembling structures of steroidal derivatives in organic solvents and their solgel transcription into double-walled transition-metal oxide nanotubes. *Journal of Materials Chemistry* **2005,** 15, (35-36), 3979-3986.

12. Schnur, J. M., Lipid tubules: a paradigm for molecularly engineered structures. *Science* **1993,** 262, (5140), 1669.

13. Larsson, S. C.; Kumlin, M.; Ingelman-Sundberg, M.; Wolk, A., Dietary long-chain n-3 fatty acids for the prevention of cancer: a review of potential mechanisms. *American Journal of Clinical Nutrition* **2004,** 79, (6), 935.

14. Op den Kamp, J. A. F., Lipid asymmetry in membranes. *Annual Review of Biochemistry* **1979,** 48, (1), 47-71.

15. Singh, A.; Price, R.; Schoen, P. E.; Yager, P.; Schnur, J. M., Tubule formation by heterobifunctional polymerizable lipids: synthesis and characterization. *Polymer Preprints* **1986,** 27, (2), 393.

16. Schnur, J. M.; Price, R.; Schoen, P.; Yager, P.; Calvert, J. M.; Georger, J.; Singh, A., Lipid-based tubule microstructures. *Thin Solid Films* **1987,** 152, (1-2), 181-206.

17. Rudolph, A. S.; Calvert, J. M.; Schoen, P. E.; Schnur, J. M., Technological development of lipid based tubule microstructures. *Advances in experimental medicine and biology* **1988,** 238, 305.

18. Rainuzzo, J. R.; Reitan, K. I.; Olsen, Y., The significance of lipids at early stages of marine fish: a review. *Aquaculture* **1997,** 155, (1-4), 103-115.

19. Balaz, S., Modeling kinetics of subcellular disposition of chemicals. *Chemical reviews* **2009,** 109, (5), 1793-1899.

www.manaraa.com

20. Enhsen, A.; Kramer, W.; Wess, G., Bile acids in drug discovery. *Drug Discovery Today* **1998,** 3, (9), 409-418.

21. Apel, C. L.; Deamer, D. W.; Mautner, M. N., Self-assembled vesicles of monocarboxylic acids and alcohols: conditions for stability and for the encapsulation of biopolymers. *Biochimica et Biophysica Acta (BBA)-Biomembranes* **2002,** 1559, (1), 1-9.

22. Bortolini, O.; Fantin, G.; Fogagnolo, M.; Maietti, S., Resolution of organic racemates via host-guest enantioselective inclusion complexation in bile acid derivatives. *Arkivoc* **2006,** 6, 40-48.

23. JiaWei, Z.; XiaoXia, Z. H. U., Biomaterials made of bile acids. *Sci China Ser B-Chem* **2009,** 52, (7), 849-861.

24. Aher, N. G., Sterioselective synthesis of steroidal side chain from 16-dehydropregnalone acetate. **2009**.

25. Li, Y.; Chu, W.; Ju, Y., Novel bile acid derived H-phosphonate conjugates: Synthesis and spectroscopic characterization. *Heteroatom Chemistry* **2008,** 19, (4), 402-407.

26. Bertolasi, V.; Ferretti, V.; Fantin, G.; Fogagnolo, M., Solid state molecular assemblies of five bile acid derivatives. *Zeitschrift Kristallographie* **2008,** 223, (8), 515-523.

27. Santra, S.; Zhang, P.; Wang, K.; Tapec, R.; Tan, W., Conjugation of biomolecules with luminophore-doped silica nanoparticles for photostable biomarkers. *Analytical Chemistry* **2001,** 73, (20), 4988-4993.

28. Resch-Genger, U.; Grabolle, M.; Cavaliere-Jaricot, S.; Nitschke, R.; Nann, T., Quantum dots versus organic dyes as fluorescent labels. *Nat Meth* **2008,** 5, (9), 763-775.

www.manaraa.com

29. Gao, X.; Cui, Y.; Levenson, R. M.; Chung, L. W. K.; Nie, S., In vivo cancer targeting and imaging with semiconductor quantum dots. *Nat. Biotechnol.* **2004,** 22, (8), 969-976.

30. Wu, X.; Liu, H.; Liu, J.; Haley, K. N.; Treadway, J. A.; Larson, J. P.; Ge, N.; Peale, F.; Bruchez, M. P., Immunofluorescent labeling of cancer marker Her2 and other cellular targets with semiconductor quantum dots. *Nat. Biotechnol.* **2003,** 21, (1), 41-46.

31. Bruchez, M., Jr.; Moronne, M.; Gin, P.; Weiss, S.; Alivisatos, A. P., Semiconductor nanocrystals as fluorescent biological labels. *Science* **1998,** 281, (5385), 2013-2016.

32. Zhong, Z.; Zhao, Y., Controlling the conformation of oligocholate foldamers by surfactant micelles. *The Journal of Organic Chemistry* **2008,** 73, (14), 5498-5505.

33. Harries, J. T.; Muller, D. P. R., Absorption of different doses of fat soluble and water miscible preparations of vitamin E in children with cystic fibrosis. *British Medical Journal* **1971,** 46, (247), 341.

34. Kobuke, Y.; Nagatani, T., Transmembrane ion channels constructed of cholic acid derivatives. *J. Org. Chem* **2001,** 66, (15), 5094-5101.

35. Miyata, M.; Tohnai, N.; Hisaki, I., Supramolecular chirality in crystalline assemblies of bile acids and their derivatives; three-axial, tilt, helical, and bundle chirality. *Molecules* **2007,** 12, (8), 1973-2000.

36. Hisaki, I.; Tohnai, N.; Miyata, M., Supramolecular tilt chirality in crystals of steroids and alkaloids. *Chirality* **2008,** 20, (3 4), 330-336.

37. Kato, K.; Inoue, K.; Tohnai, N.; Miyata, M., Helical tape assemblies in inclusion crystals of bile acids and their derivatives. *Journal of Inclusion Phenomena and Macrocyclic Chemistry* **2004,** 48, (1), 61-67.

www.manaraa.com

38. Sada, K.; Sugahara, M.; Kato, K.; Miyata, M., Controlled expansion of a molecular cavity in a steroid host compound. *J. Am. Chem. Soc* **2001,** 123, (19), 4386-4392.

39. Watabe, T.; Kato, K.; Tohnai, N.; Miyata, M., An approach to the Qualitative Prediction of Crystal Structures; Hierarchical Crystal Structures of Inclusion Compounds of Steroids and Alkaloids. *Structure and Dynamics in Macromolecular Systems with Specific Interactions*, 157?67.

40. Zastavker, Y. V.; Asherie, N.; Lomakin, A.; Pande, J.; Donovan, J. M.; Schnur, J. M.; Benedek, G. B., Self-assembly of helical ribbons. *Proceedings of the National Academy of Sciences of the United States of America* **1999,** 96, (14), 7883.

41. Babu, P.; Sangeetha, N. M.; Maitra, U. In *Supramolecular chemistry of bile acid derivatives: formation of gels*, 2006; Wiley Online Library: 2006; pp 60-67.

42. Sangeetha, N. M.; Maitra, U., Supramolecular gels: Functions and uses. *Chemical Society Reviews* **2005,** 34, (10), 821-836.

43. Nonappa, U. M., Unlocking the potential of bile acids in synthesis, supramolecular/materials chemistry and nanoscience. *Org. Biomol. Chem.* **2007**.

44. Virtanen, E.; Kolehmainen, E., Use of bile acids in pharmacological and supramolecular applications. *European Journal of Organic Chemistry* **2004,** 2004, (16), 3385-3399.

45. Monte, M. J.; Marin, J. J. G.; Antelo, A.; Vazquez-Tato, J., Bile acids: chemistry, physiology, and pathophysiology. *World Journal of Gastroenterology: WJG* **2009,** 15, (7), 804.

46. Salunke, D. B.; Hazra, B. G.; Pore, V. S., Steroidal conjugates and their pharmacological applications. *Current medicinal chemistry* **2006,** 13, (7), 813-847.

www.manaraa.com

CHAPTER 2: ASSEMBLY OF VESICLES INTO FRACTAL AND PRONG PATTERNS ON SUBSTRATES

2.1 Introduction

Spherical vesicles of surfactants are unique building blocks. Control over the assembly of them into higher order structures may aid in the creation of new soft materials that are important from both technological and fundamental standpoints. Molecular self-assembly based on cooperative weak interactions is a powerful strategy for synthesizing technically useful supramolecular structures with well-defined sizes and shapes in solution.[1-2] Spherical vesicles are one of well-known supramolecular structures formed by the self-assembly of surfactants.[3] Progress has been made in developing their applications as vehicles for drug delivery [3] and reaction vessels for charge storage,[4] signal amplification,[5] energy transport,[6] and chemical compound mixing.[7]

In recent years, there has been growing interest in using spherical vesicles as building blocks to assemble higher-order structures for designing new soft materials. It has been shown that some surface functionalized vesicles can undergo a secondary self-assembly into three-dimensional multivesicle aggregates by electrostatic and ligand-receptor interactions [8-13] or one-dimensional tubular structures by fusion of linear aggregated vesicles.[14-16].

We found that fractal assemblies of lithocholic acid (LCA) vesicles on glass slides by diffusion-limited aggregation. With the use of capillary flow generated in an evaporating vesicle solution confined by two parallel glass slides, we are able to assemble LCA vesicles into pronglike structures. The fusion of linear aggregated LCA vesicles within these assemblies can

www.manaraa.com

lead to the formation of fractal and prong patterns of LCA tubes. We show that vesicles of lithocholic acid (LCA), which adsorb on glass slides from solution, can assemble into two-dimensional fractal patterns by diffusion-limited aggregation. By using capillary flow generated in an evaporating vesicle solution between two glass slides, we are able to assemble LCA vesicles into prong patterns. The fusion of assembled LCA vesicles leads to the formation of fractal and prong patterns of LCA tubes.

2.2 Experimental and methods

2.2.1 Synthesis of LCA vesicless

Lithocholic acid (LCA) was purchased from Aldrich and used without further purification. Water used in our experiments was purified with an Easypure II system (18 MΩ cm, pH 5.7). Microscope cover glass slides were purchased from Fisher Scientific. The formation of LCA vesicles in aqueous solution was conducted at room temperature. First, 30 mg of LCA was added to 10 mL of water. The pH of LCA solution was adjusted to 12.0 by adding NaOH. The LCA solution was vortexed for 2 min and then kept in a sealed glass vial at room temperature. A dipping machine of Langmuir-Blodgett trough (NIMA Technology) was used to withdraw vertically glass slides from vesicle solution. An Olympus BX40 optical microscope equipped with a digital camera (Olympus C2020 Zoom) was used to observe the adsorption and assembly of vesicles on glass slides. Fourier transform-infrared (FT-IR) spectra of LCA vesicles dried on an ATR crystal were recorded with a Perkin-Elmer (100) spectrometer operating at 4 cm^{-1} resolution.

www.manaraa.com

2.3 Results and discussion

2.3.1 Structure change vesicles

Lithocholic acid (LCA) is a biologically active surfactant. It has been shown that the self-assembly behavior of LCA is very sensitive to the conditions under which self-assembly occurs.[16-19] At pH 12.0, we find that the LCA can form spherical vesicles with a uniform diameter of ~ 1.5 μm (Figure 2.1a), which are much larger than the micelles of cholic and decoxycholic acids formed by small numbers of molecules (four to ten).[20-21] All LCA vesicles shown in Figure 1a have a low contrast region at the center, which suggests that they are a hollow structure. Fourier transform-infrared spectrum of LCA vesicles reveals two absorption peaks at 2930 cm^{-1} and 2864 cm^{-1} in the range from 2800 cm^{-1} to 3000 cm^{-1}. These two peaks represent the asymmetric and symmetric stretching vibration of the CH_2 in the short acyl chain of LCA molecules. In the carbonyl stretching region, the weak peak at 1700 cm^{-1} can be assigned to the C=O stretching vibration of the COOH group, while the strong absorption peak at 1570 cm^{-1} is a result of the stretching vibration of the COO^- group, suggesting that the LCA molecules in spherical vesicles are partially deprotonated.

www.manaraa.com

We find that LCA vesicles are able to assemble into two-dimensional fractal patterns on glass substrates through diffusion-limited aggregation. In our experiments, a glass slide was immersed in freshly prepared vesicle solution. After a short period of immersion time, the glass

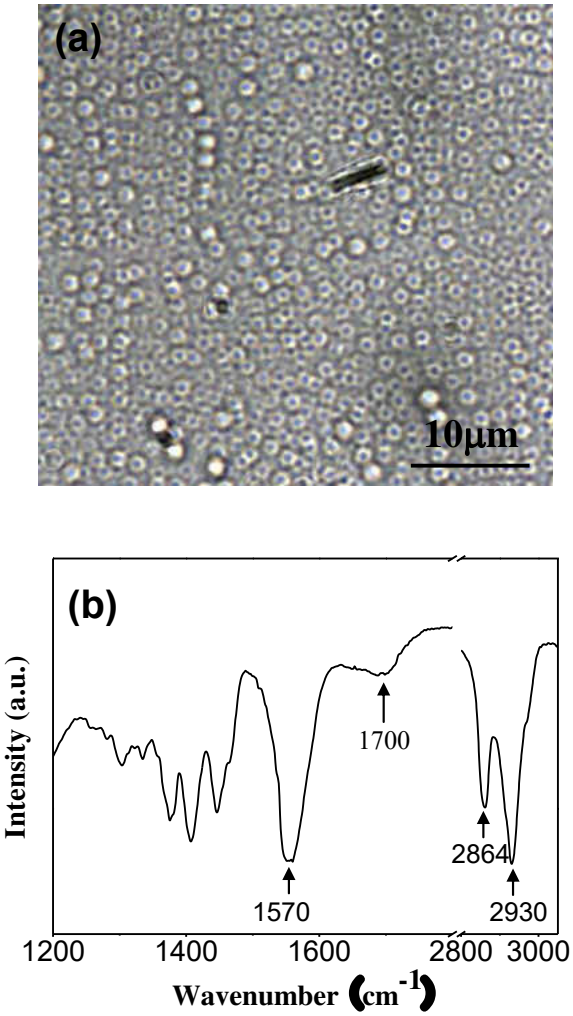

Figure 2.1 (a) Optical microscopy image of self-assembled LCA vesicles in aqueous solution at pH of 12.0. (b) FT-IR spectrum of LCA vesicles dried on an ATR crystal.

slide was vertically withdrawn at a speed of 1 mm/min with a dipping machine of Langmuir-Blodgett trough and then examined by an optical microscope. Figure 2 shows optical microscopy images of glass slides immersed in vesicle solution for different periods of time.

www.manaraa.com

After 15 min immersion, we observe the adsorption of individual vesicles on glass slides (Figure 2.2a). As more vesicles adsorb on glass substrates over time, they form small aggregates with fractal patterns (Figure 2.2b). Each fractal contains a center at which a single vesicle (seed) is

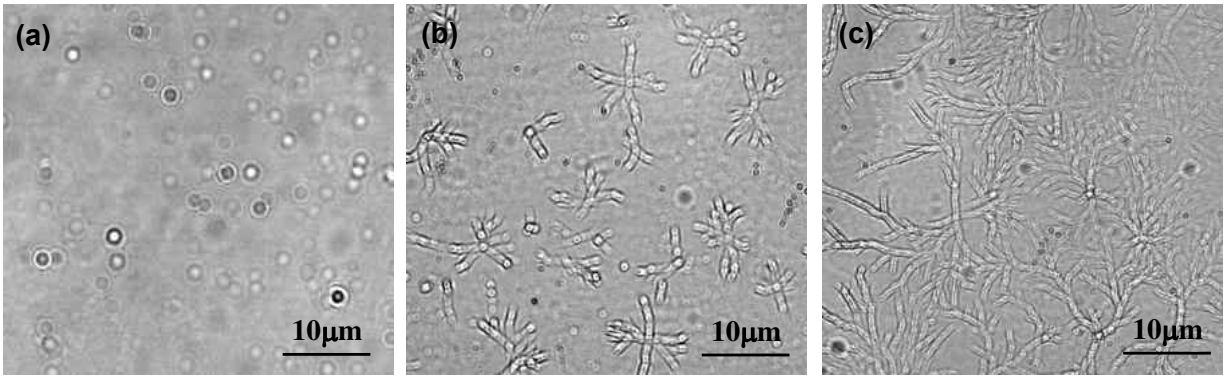

Figure 2.2 Optical microscopy images of a fractal assemble of LCA vesicles on glass slides by diffusion-limited aggregation. These glass slides were immersed in vesicle solution for 15 mins (a), 120 mins (b) and 24 hours. These images were taken immediately after glass slides were withdrawn from vesicle solution.

located and several branches in which several vesicles are linearly aggregated. Longer time immersion leads to the growth of fractal patterns by increasing the number of branches (Figure 2.2c). As a control, we simply dried a droplet (50 μL) of vesicle solution with the same concentration on a glass slide in air at room temperature. The drying process was often completed within 15 min. We find no fractal patterns formed from the fast dried sample.

2.3.2 Fractal growth of vesicles

Figure 3a is an optical microscopy image of fractal assembles of vesicles on a glass slide after 12 hour immersion. Compared to the fractals formed with short time immersion (Figure 2.2b), the fractal structures formed with longer time immersion are significantly larger and

www.manaraa.com

composed of a large number of vesicles. The formation of these large fractal assemblies is often accompanied by the complete disappearance of individual vesicles around them. As can be seen from the enlarged image inset in Figure 2.3a, with longer time immersion the linearly aggregated vesicles within the branches start to fuse into tube structures. The continuous dark line represents the inner cavity of the tubes. When viewed between crossed polarizers, the two-dimensional fractal patterns of tubes exhibit birefringence (Figure 2.3b), suggesting that they have an extended crystalline structure. The dimension of the fractal pattern was calculated

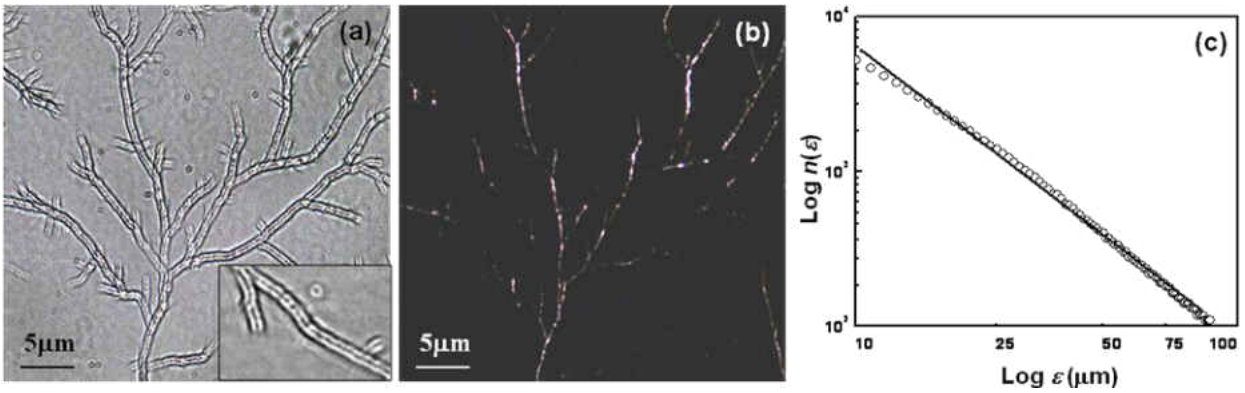

Figure 2.3 Optical (a) and polarizing (b) microscopy images of a fractal pattern of LCA vesicles on a glass slide. The enlarged image of the branches of the fractal pattern was inset in Figure 3a. (c) Box-counting calculation of the fractal pattern. The slope of the linear fitting of the log-log plot of n(ε) versus ε is -1.746.

using the box-counting method.[22] The number of boxes of size ε which contain a portion of the fractal, n(ε), scales as $n(\varepsilon) \sim \varepsilon^{-D}$ over a range of values of ε, where D is fractal dimension which is given by the slope of the log-log plot of n(ε) versus ε. Figure 2.3c shows the plot of log n(ε)

www.manaraa.com

versus log ε for the fractal pattern in Figure 2.3a. The dimension D of the fractal pattern is calculated to be 1.746.

Instead of immersing glass slides in vesicle solution, we confined vesicle solution with two parallel glass slides. We find that capillary flow generated in the confined vesicle solution is able to assemble LCA vesicles into linear arrays and prong like structures. In this experiment, 50 μL of LCA vesicle solution was added on a glass slide and then another glass slide was placed on it. The vesicle solution confined between the two glass slides spread into a thin film to balance the weight on top of it. The thickness of the confined vesicle solution was estimated to be ~ 15 μm at initial stages. The evaporation of the confined vesicle solution causes the receding of contact line. Over time, we note that micron sized channels extend from the receding contact line (Figure 2.4). They grow perpendicular to the contact line. The growth rate of the channels is estimated to be about 0.6 μm/s. We find that the capillary flow generated by the pressure gradient due to the parabolic shape of the contact line near the channel is able to pull vesicles into the channel. Scherer and coworkers suggest that the stability of the channels grown from the receding contact line of thin liquid films between two glass slides is a result of the adsorption of surfactants at the air-liquid interface.[23] The channel growth will lead to the increase of interface area, while surface tension opposes this change. In the presence of surfactants in solution, the increase of interface area is accompanied by the diffusion of surfactants from the solution to the interface, which can compensate the energy loss due to the area increase, making the channel growth more energetically favorable. In our case, we expect that the adsorption of excess LCA molecules from the vesicle solution to the air-liquid interface prevent the channels from collapsing. A control experiment was carried out to verify the proposed mechanism. We purified LCA vesicles by centrifuging vesicle solution to remove excess

www.manaraa.com

LCA monomers in vesicle solution and then resuspend the purified vesicles in pure aqueous solution. The pure aqueous solution confined by two parallel glass substrates does not form stable channels during the receding of contact line.

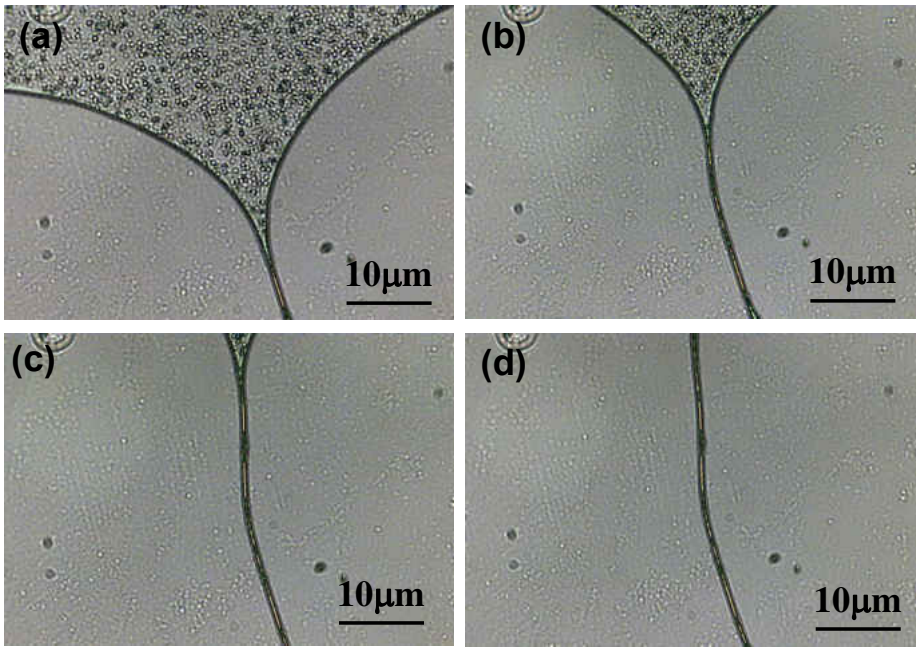

Figure 2.4 Optical microscopy images of the growth of a micron sized channel from the receding contact line of the vesicle solution confined by two parallel glass slides. Time interval of these images was 2 seconds. The vesicles pulled into the channel by capillary flow.

2.3.3 Surface tention induced vesicles arrangement

www.manaraa.com

We find that each channel starts with a small clump in which vesicles aggregate, producing

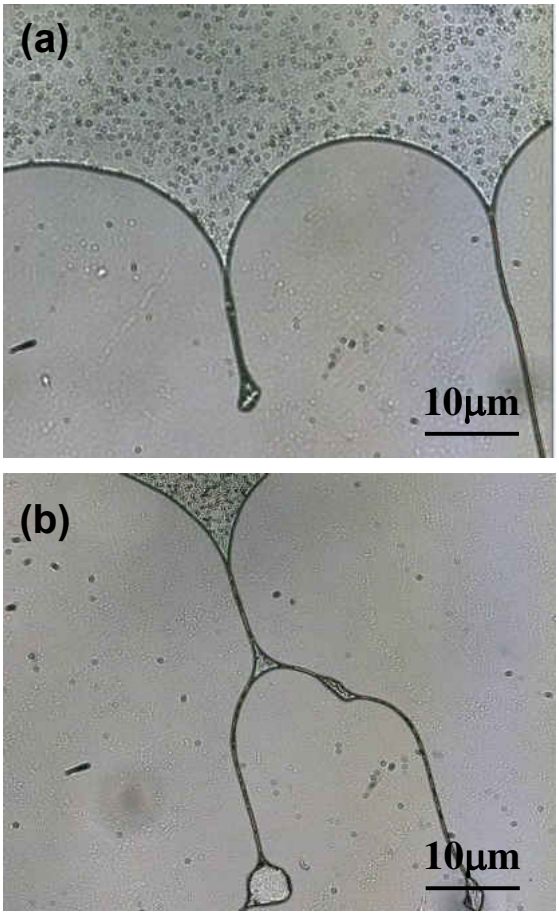

Figure 2.5 (a) Optical microscopy image of two parallel channels with a clump made of vesicle aggregates at their ends. The clump acts a pinning point at which each channel starts. (b) Optical microscopy image of two parallel channels that are forced together by the nonuniform motion of the receding contact line to form a prong like pattern.

a pinning point (Figure 2.5a). Multiple channels can grow from the same receding contact line. The spacing between them depends on the positions of the pinning points formed at the contact line boundary. The nonuniform motion of the receding contact line can force two nearby channels

www.manaraa.com

to meet and coalesce into a prong like structure (Figures 2.5b). Since the vesicle solution in the channels is constantly evaporating, a new supply of vesicle solution must be maintained to prevent channels from drying up. We find that the channels collapse if they are broken off from the contact line boundary. When the two glass surfaces are peeled apart, parallel arrays (Figure 2.6a) and prong like assemblies (Figure 2.6b) of vesicles are left on one glass slide.

Interestingly, if the samples are kept in a humidity chamber for days, we find that the linear aggregates of LCA vesicles in these higher order assemblies on glass substrates are able to fuse

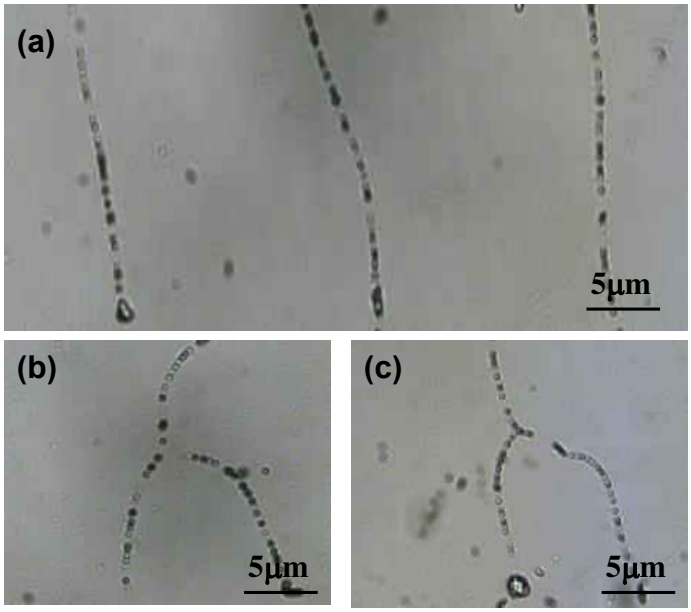

Figure 2.6 Optical microscopy images of parallel arrays (a) and prong like patterns (b and c) of LCA vesicles assembled on glass substrates.

into tube like structures, leading to the formation of fractal and prong patterns of LCA tubes (Figure 2.7). Recently, great efforts have been made in constructing ordered arrays of surfactant tubes. For example, Orwar and co-workers [24] reported the formation of ordered tube arrays by

www.manaraa.com

wiring the fluidic tubes, which are pulled from lipid vesicles, around microfabricated SU-8 pillars with a micropipet technique. Brazhnik et al.[25] and Dittrich et al.[26] use the direct self-assembly of surfactants within microfluidic channels to form bundles of aligned tubes. Shimizu and collaborators [27] described an approach in which tubes of cardanyl β-**d**-glucopyranoside were aligned by microextruding an aqueous dispersion onto a glass substrate with a needle. In previous publications, we reported the formation of two-dimensional arrays of aligned 1,2-bis(tricosa-10,12-diynoyl)-sn-glycero-3-phosphocholine tubules on substrates using

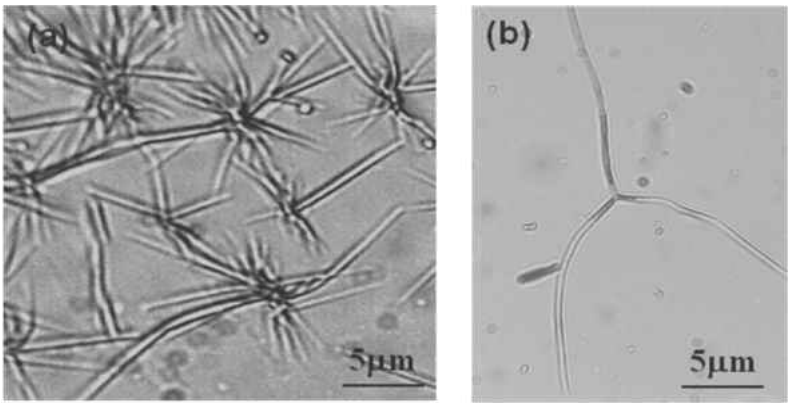

Figure 2.7 Optical microscopy images of fractal (a) and prong like patterns (b) of LCA tubes formed by fusion of linearly aggregated LCA vesicles in small fractals and channels on glass substrates.

microfluidic networks,[28] moving contact lines,[29] or microcontact printing.[30] The method described here provides a new approach to assemble more complex patterns of tubes.

2.4 Conclusions

In conclusion, we have shown a fractal self-assembly of LCA vesicles on glass substrates by diffusion-limit aggregation. Each branch of fractal patterns consists of linearly aggregated LCA vesicles. The capillary flow generated in an evaporating vesicle solution confined by two parallel glass slides allows us to assemble LCA vesicles into parallel arrays and prong like

www.manaraa.com

patterns. The fusion of linear aggregated LCA vesicles in these assembles can lead to the formation of complex patterns of LCA tubes. The methods described here open up new avenues for controlling the long-range assembly of vesicles and tubes on substrates into well-defined patterns, which are critical in developing their applications as a new type of soft materials.

2.5 References

1. Lehn, J. M., Toward complex matter: Supramolecular chemistry and self-organization. *Proc. Natl. Acad. Sci. U.S.A.*, **2002**, 99, 4763.

2. Whitesides, G. M. and Grzybowski, B., Self-assembly at all scales. *Science*, **2002**, 295, 2418.

3. Ringsdorf, H.; Berhard, S. and Venzmer, J., Hermann Staudinger and the future of polymer research jubilees- Beloved occasions for cultural piety. *Angew. Chem. Int. Ed. Engl.*, **2004**, 43, 1064.

4. Stanish, I.; Lowy, D. A.; Lee, Y.; Fang, J. Y.; Wong, E.; Ray, R.; and Sing, A., Structural and electrochemical characterization of immobilized polymerized electroactive vesicles. *J. Phys. Chem. B.*, **2004**, 108, 127.

5. Bolinger, P. Y.; Stamou D.; and Vogel. H., Integrated nanoreactor systems: Triggering the release and mixing of compounds inside single vesicles. *J. Am. Chem. Soc.*, **2004**, 126, 8594.

6. Khairutdinov, R. F. and Hurst, J. K., Cyclic transmembrane charge transport by pyrylium ions in a vesicle-based photocatalytic system. *Nature*, **1999**, 402, 509.

7. Gust, D.; Moore T. A. and Moore, A. L.; Mimicking photosynthetic solar energy transduction. *Acc. Chem. Res.*, **2001**, 34, 40.

www.manaraa.com

8. S. Chiruvolu, S.; Walker, J.; Israelachvili, F.; Schmitt, J.; Leckband, D. and Zasadzinski, J. A, Higher-order slef-assmebly of vesicles by site-specific binding. *Science*, **1994**, 264, 1753.

9. Kisak,E. T.; Kennedy, M. T.; Trommeshauser, D. and Zasadzinski, J. A., Self-limiting aggregation by controlled ligand-receptor stoichiometry. *Langmuir*, **2000**, 16, 2825.

10. P. Vermette, S. Taylor, D. Dunstan and Meagher, L., Control over PEGylated-liposome aggregation by NeutrAvidin-biotin interactions investigated by photon correlation spectroscopy. *Langmuir*, **2002**, 18, 505.

11. Sideratou, Z.; Foundis, J.; Tsiourvas, D.; Nezis, I. P.; Papadimas, G. and Paleos, C. M., A novel dendrimeric "glue" for adhesion of phosphatidyl choline-based liposomes. *Langmuir*, **2002**, 18, 5036.

12. Wu, C. M.; Chen, H. L.; Liou, W.; Lin, T. L. and Jeng, U. S., DNA-induced aggregation of zwitterionic oligolamellar liposome. *Biomacromolecules*, **2004**, 5, 2324.

13. Tsogas, I.; Tsiourvas, D.; Nounesis, G. and Paleos, C. M.; Interaction of poly-L-arginine with dihexadecyl phosphate/phosphatidylcholine liposomes. *Langmuir*, **2005**, 21, 5997.

14. Lauf, U.; Fahr, A.; Westesen, K. and Ulrich, A. S., Novel lipid nanotubes in dispersions of DMPC. *ChemPhysChem.*, **2004**, 5, 1246.

15. Tellini, V. H.; Jover, S. A.; Meijide, F.; Tato, J. V.; Galantini, L. and Pavel, N. V., Supramolecular structures generated by a p-tert-butylphenyl-amide derivative of cholic acid: From vesicles to molecular tubes. *Adv. Mater.*, **2007**, 19, 1752.

16. Zhang, X.; Zou, J.; Tamhane, K.; Kobzeff, F. F. and Fang J. Y., Self-Assembly of pH-Switchable Spiral Tubes: Supramolecular Chemical Springs. *Small*, **2010**, 6, 217.

www.manaraa.com

17. Tan, Y. C., Shen, A. Q.; Li, Y.; Elson, E. and Ma. L., Engineering lipid tubules using nano-sized building blocks: the combinatorial self-assembly of vesicles. *Lab Chip.*, **2008**, 8. 339.

18. Terech, P. and Talmon, Y., Aqueous suspensions of steroid nanotubules: Structural and rheological characterizations. *Langmuir*, **2002**, 18, 7240.

19. Pal, A.; Basit, H.; Sen, S.; Aswal, V. K. and Bhattacharya, S., Structure and properties of two component hydrogels comprising lithocholic acid and organic amines. *J. Mater. Chem.*, **2009**, 19, 4325.

20. Tamhane, K.; Zhang, X.; Zou, J. and Fang, J. Y., Assembly and disassembly of tubular spherulites. *Soft Matter*, **2010**, 6, 1224.

21. Oakenfull, D. G. and Fisher, L. R., Role of hydrogen-bonding in formation of bile-salt micelles. *J. Phys. Chem.*, **1977**, 81, 1838.

22. Venkatesan, P.; Cheng, Y. and Kahne, D., Hydrogen-bonding in micelle formation. *J. Am. Chem. Soc.*, **1994**, 116, 6955.

23. Vicsek, T., Fractal growth phenomena. *World Scientific*, Singapore, **1992**.

24. Vyawahare, S.; Craig, K. M. and Scherer, A., Patterning lines by capillary flows. *Nano Lett.*, **2006**, 6, 271.

25. Hurtig, J.; Gustafsson, B.; Tokarz, M.; Orwar, O., Electrophoretic transport in surfactant nanotube networks wired on microfabricated substrates. *Anal. Chem.*, **2006**, 78, 5281.

26. Brazhnik, K. P.; Vreeland, W. N.; Hutchison, J. B.; Kishore, R.; Well, J.; Helmerson, K. and Locascio, L. E., Directed growth of pure phosphatidylcholine nanotubes in microfluidic channels. *Langmuir*, **2005**, 21, 10814.

www.manaraa.com

27. Dittrich, P. S.; Heule, M.; Renaud, P. and Manz, A., On-chip extrusion of lipid vesicles and tubes through microsized apertures. *Lab Chip.*, **2006**, 6, 488.

28. Frusawa, H.; Fukagawa, A.; Ikeda, Y.; Araki, J. A.; Ito, K.; John, G. and Shimizu, T., Aligning a single-lipid nanotube with moderate stiffness. *Angew. Chem. Int. Ed.*, **2003**, 42, 72.

29. Mahajan, N. and Fang, J. Y., Two-dimensional ordered arrays of aligned lipid tubules on substrates with microfluidic networks. *Langmuir*, **2005**, 21, 3153.

30. Zhao, Y. and Fang, J. Y., Hermann Staudinger and the future of polymer research jubilees-Beloved occasions for cultural piety. *Langmuir*, **2006**, 22, 1891-1895.

31. Fang, J. Y., Ordered arrays of self-assembled lipid tubules: fabrication and applications. *J. Mater. Chem.*, **2007**, 17, 3479.

32. Zhao, Y. and Fang, J. Y., Direct printing of self-assembled lipid tubules on substrates. *Langmuir*, **2008**, 24, 5113.

www.manaraa.com

CHAPTER 3: SELF-ASSEMBLY OF pH-SWITCHABLE SPIRAL TUBES: SUPRAMOLECULAR CHEMICAL SPRINGS

3.1 Introduction

Helical structures are commonly found in nature at different length scales.[1-2] Perhaps the most notable examples are simple α-helical peptides, double helical nucleic acids, triple helical collagens, and more complex helical microtubules and tobacco mosaic virus. These helical structures in nature have captivated the minds of scientists over decades because they are associated with many biological events. It is known that these biological helical structures, such as collagens, microtubules and viruses are formed by the self-assembly of basic building blocks (protein subunits). Inspired by the synthetic strategy in nature, great efforts have been made in synthesizing helical supramolecular structures with controlled morphologies and helicities by the self-assembly of synthetic small molecules because of their potential applications in materials science and enantioselective catalysis.[3-4]

The self-assembly of chiral amphiphilic molecules in aqueous solutions is of particular interest because the chirality of individual molecules is often expressed in their supramolecular structures. For example, a number of synthetic chiral amphiphilic molecules have shown the ability of self-assembling into helical ribbons in aqueous solutions. These include carbohydrate amphiphiles,5-8 amino acid-based amphiphiles,[9-13] peptide amphiphiles,[14-17] diacetylenic lipids,[18-20] gemini surfactants,[21-22] nucleotide-based amphiphiles,[23-25] and bile acids.[26-29] Interest in the self-assembly of helical ribbons is driven by not only the fundamental understanding of the relationship between molecular chirality and supramolecular chirality but also their material

www.manaraa.com

applications. In many cases, the self-assembled helical ribbons are metastable. The closing of the gaps of the helical ribbons can lead to the formation of rigid and straight tubes.

Herein, we report the self-assembly of lithocholic acid (LCA) tubes in aqueous solution with pH 12.0 at room temperature. The self-assembled LCA tubes can coil into a spiral shape, and then transit into a straight shape as the pH of solution is reduced from 12.0 to 7.4 with hydrogen chloride (HCl). The shape transition of LCA tubes is reversible when the pH of solution is adjusted back to 12.0 by adding sodium hydroxide (NaOH).

3.2 Experimental and methods

3.2.1 Synthesis of LCA tubes

Lithocholic acid (98%) from Aldrich was used as received. We dispersed 30 mg of the LCA in 10 mL of water with the addition of 0.1M sodium hydroxide (NaOH) to adjust the pH of aqueous solutions to 12.0 at room temperature (23°C). The solutions were then vortexed for 2 min and stored in glass vials with a sealed top at 23 °C.

The solubility of the LCA in aqueous solution can be improved by raising the pH. In our experiments, 30 mg of the LCA was added to 10 mL of water with 0.1M NaOH. The LCA was completely soluble in this alkaline aqueous solution with pH 12.0. The LCA solution was vortexed for 2 min and then kept in a sealed glass vial at room temperature for different periods of time. A drop (~ 100 μL) of the solution was placed on a glass substrate and then observed with an optical microscope.

www.manaraa.com

3.2.2 Characterization

The self-assembled supramolecular structures in solutions at different pH values were observed by Olympus BX40 microscope with a digital camera (Olympus C2020 Zoom). X-ray diffraction (XRD) patterns of LCA tubes dried on glass substrates were recorded with a Rigaku D/max diffractometer with CuKa radiation (λ = 1.542 Å) operated at 40 kV and 30 mA. An atomic force microscope (AFM) (Dimension 3100, Digital Instruments) with a built-in optical microscope was used to cut the tubes absorbed on glass slides in aqueous solution at different pH values. A silicon nitride cantilever (Nanosensors) with a spring constant of 0.051 N/m (given by the manufacturer) was used in cutting the tubes under contact mode by scanning them in a line. The size of the cantilever tips (radius of curvature) is about 15 nm according to the manufacturer. The Fourier transform infrared spectra (FT-IR) of tube were recorded by a Perkin-Elmer (Spectrum 100) spectrometer equipped with an ATR sampling accessory. Transmission electron microscopy measurements of tubules dried on carbon-coated grids were performed on a Tecnai F30 microscope with an accelerating voltage of 300kV.

3.3 Results and discussion

3.3.1 Growth of LCA tube in solution

www.manaraa.com

We find that the LCA molecules form vesicles with an external diameter of ~ 1.5 μm after 2 hours (Figure 3.1b). The self-assembled vesicle structure is different from the reported small

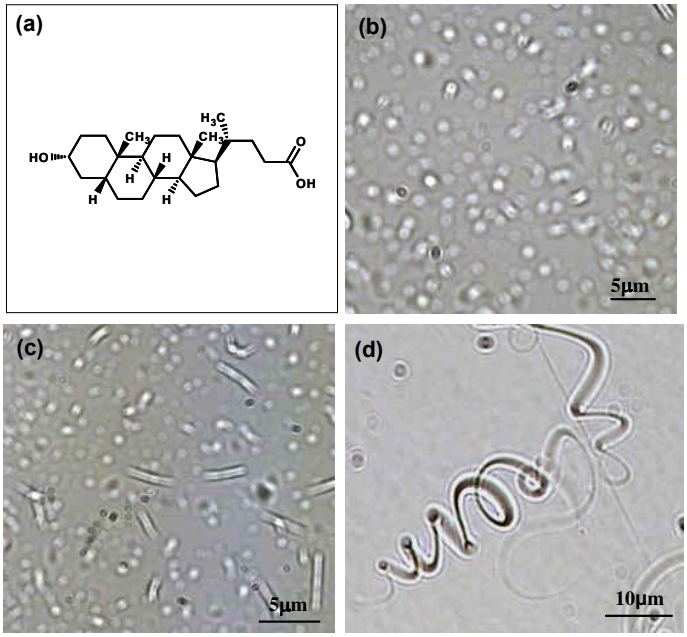

Figure 3.1 (a) Chemical structure of lithocholic acid. Optical microscopy images of self-assembled structures of LCA molecules in alkaline solution (pH 12.0) at room temperature after 2 hours (b), 6 hours (c), and 3 days (d).

aggregates (called micelles) formed by some of other bile salts through the back-to-back hydrophobic interactions between the convex sides, with the hydrophilic concave side pointing outward in water.[31-32] The hollow core of self-assembled vesicles is clearly visible in Figure 3.1b. The initially formed vesicles linearly aggregate with time. The fusion of these linearly aggregated vesicles leads to the formation of hollow cylindrical tubes (Figure 3.1c). Eventually, these trapped vesicles in the tubes disappear, possibly being integrated into the tube walls and becoming part of

www.manaraa.com

the tubes. The self-assembled mechanism of LCA tubes differs from that of other bile acid tubes in which the helical ribbons are a precursor.[26-29] We find that the LCA tubes continuously grow until all vesicles are consumed. Interestingly, the LCA tubes coil into 3D spirals as their lengths increase (Figure 3.1d). The coiling of LCA tubes is a slow process and takes a few days to

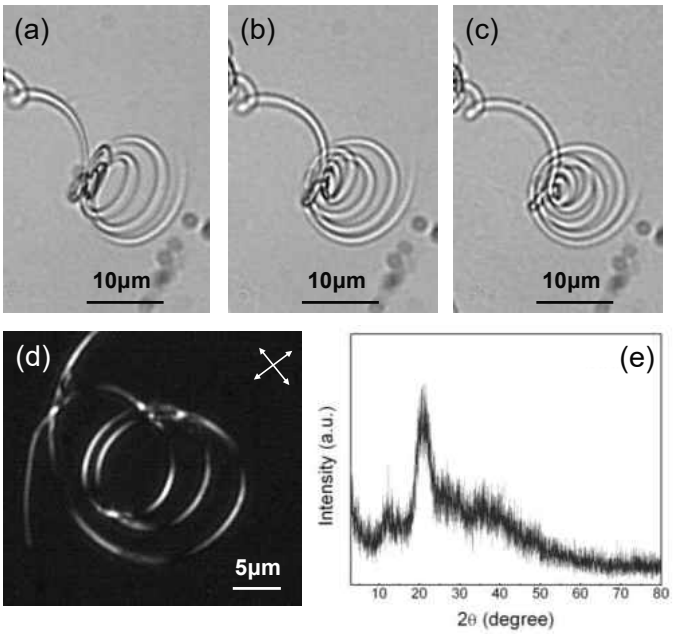

Figure 3.2. (a-c) Optical microscopy images of the deposition process of a 3D left-handed spiral tube on a glass substrate during water evaporation in air. (d) Polarizing microscopy image of a 3D spiral tube in aqueous solution. (e) X-ray diffraction of spiral tubes dried on a glass substrate. The direction of the polarizer and analyzer is indicated by while arrows in (d).

complete. However, due to Brownian motion and convection, it is difficult to track the coiling process of a single tube over days. The change in the apparent diameter of the spiral tubes is a result of the defocus under optical microscope.

The handedness of 3D spiral tubes is difficult to be determined by an optical microscope since their apparent handedness changes during a through-focus imaging. We find that the 3D spiral tubes gradually deposit on the glass substrate and contract into 2D spirals with water

www.manaraa.com

evaporation (Figure 3.2). In this case, the handedness of spiral tubes can be unambiguously determined by positioning the microscope objective focal plane at the substrate. All spiral tubes are found to be left-handed. The microscopic handedness of spiral tubes should be tied to the intrinsic chirality of the steroid nucleus of the LCA. It is also clear from the optical contrast of the microscopy image shown in Figure 3.2 that what we observe is spiral tubes rather than spiral ribbons, based on their optical contrast. Optical microscopy images are known to be the 2D projection of objects in focus. Ribbons should have a uniform optical contrast throughout, while tubes in the 2D projection should show optical contract between the tube walls and the inner aqueous core. The relatively bright center represents the inner aqueous core. The two parallel dark edges represent both sides of tube walls. It is not clear why the tubes coil into spirals rather than helices. We speculate that the formation of spirals may be the result of the gradual change in the tubular diameter and/or wall thickness from one end of the tubule to the other. When viewed between crossed polarizers, the spiral LC tubes exhibit a Maltese-cross extinction pattern (Figure 2d). The observed birefringence suggests that the spiral tubes have an extended crystalline structure. The characterization of the molecular packing within the spiral tubes was carried out by using wide-angle x-ray diffraction. The x-ray diffraction pattern (Figure 3.2e) shows two well-resolved reflections at $2\theta = 11.8°$ and 21°, corresponding to a *d* spacing of 7.45 Å and 4.22 Å, respectively.

We find that not all LCA tubes are able to coil into spiral shapes within a week. The LCA tubes with large diameters are uncoiled. However, they are metastable and have a tendency to disassemble into several small tubes after aging in aqueous solution at room temperature for a month. The disassembly starts at the tube ends (Figure 3.3a). The small tubes gradually coil into

www.manaraa.com

spirals in aqueous solution with one end still attached to the large uncoiled tubes (Figure 3.3b). The growth of small spiral tubes is analogues to that of left-handed helix of tendrils of climbing plants.

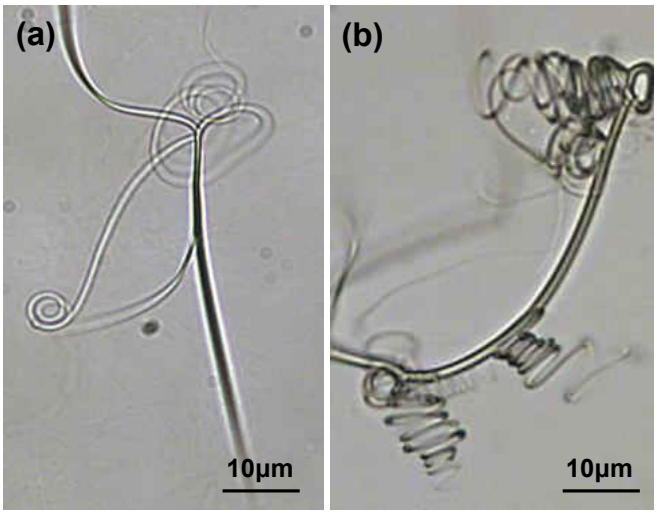

Figure 3.3 (a-b) Optical microscopy images of disassembly of large tubes in aqueous solutions at pH 12.0 after a month. The separated small tubes coil into spiral shapes.

With time, these spiral tubes completely separate from the large uncoiled tubes.

3.3.2 Conformation change triggered by pH value

The spiral tubes are stable in aqueous solution at pH 12.0. However, as the pH of solution is reduced from 12.0 to 7.4 by adding HCl, we find that they transit into a straight shape (Figures 3.4a and 3.4b). The uncoiling process of LCA tubes at the early stage is too fast to be resolved in our experimental setup. Therefore, how the left-handed spiral tubes are unzipped is unknown. However, when the pH of solution is adjusted back to from 7.4 to 12.0 by adding NaOH, the straight tubes switch back to the spiral shape. The structure of straight tubes was further characterized with a transmission electron microscope (TEM).

www.manaraa.com

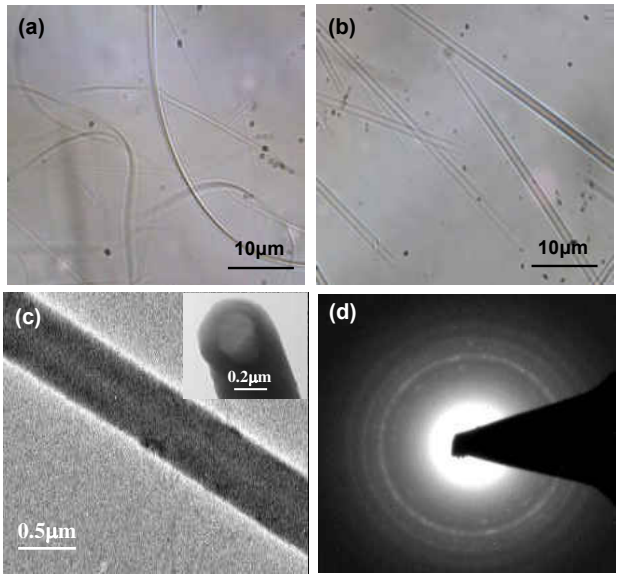

Figure 3.4 (a-b) Optical microscopy images of the shape transition of coiled tubes in aqueous solutions when the pH was reduced from 12.0 to 7.4. The images were taken after adding HCl for 1 min (a) and 3 min (b). (c) TEM image of a straight tube dried on a carbon-coated grid. The TEM image of the end of a tube is inset in (c). (d) Electron diffraction pattern of tube walls. The TEM measurements were carried at room temperature.

Figure 4c presents a typical TEM image of a straight LCA tube with an external diameter of ~ 0.6 μm. The hollowness of the tube is visible from the TEM image, which shows a contrast of electron density between the light central channel and the dark walls. The wall thickness is measured to be ~ 0.2 μm. The hollowness of straight LCA tubes is further confirmed by examining their ends with TEM (see in the inset in Figure 3.4c). It is also clear from the TEM image that the hollow LCA tube has an open end. The electron diffraction from the tube wall shows concentric rings (Figure 3.4d), suggesting that the LC tube has a polycrystalline structure.

Recently, mesoscale simulations have shown that the shape of self-assembled supramolecular structures of chiral molecules is determined by the balance between their elasticity and chirality.[34] The shape transition of one-dimensional chiral aggregates can be achieved by

www.manaraa.com

varying their elastic modulus. In our case, we expect that the chiral interaction of the steroid nucleuses is the main driving force for the coiling of LCA tubes. The hydrophobic and electrostatic interactions of LCA molecules are expected to contribute the elastic properties of LCA tubes. The

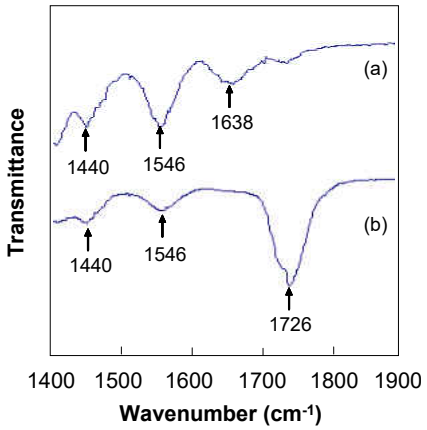

Figure 3.5. FT-IR spectra of spiral (a) and straight (b) tubes dried on an ATR crystal.

formation of spiral tubes suggests that the chiral interaction provides sufficient energy to compensate the elastic penalty for coiling tubes. Any external stimulus that disrupts the elastic modulus of LCA tubes will break the balance, leading to the shape transition.

It is well established that the ionization constant of the COOH groups of LCA depends on the local environment. The pK_a value of the LCA is 7.0 ~ 8.4 in crystalline monolayers.[35] Therefore, as the pH of solutions is reduced from 12.0 to 7.4, a relatively large amount of the LCA molecules are expected to be deprotonated in the tube walls, which is evident from the Fourier transform-infrared (FT-IR) spectra (Figure 3.5). The main discrepancy of absorption peak positions between the spiral (Figure 3.5a) and the straight (Figure 3.5b) tubes is in the region from 1600 cm^{-1} to 1800 cm^{-1}. The absorption peak of spiral tubes at 1638 cm^{-1} can be assigned to the stretching vibration of the COO^{-} group of the LCA salt, while for the straight tubes, the stretching

www.manaraa.com

vibration of the COO^- group is diminished. A strong absorption peak at 1726 cm^{-1} assigned to the C=O stretching vibration of the COOH group appears, suggesting that the LCA molecules are deprotonated in the straight tubes. In addition, the position of the C=O stretching vibration at 1726 cm^{-1} suggest the formation of hydrogen bonding (COOH-HOOC) between two LCA molecules at the straight tubes.[36]

3.2.3 Mechanic property of LCA tube

The strong hydrogen bonding of the LCA molecules will reduce their mobility and strengthen the LCA tubes. To test this hypothesis, we studied the mechanical strength of LCA tubes at different pH values under applied load with an atomic force microscope (AFM) tip. Both the spiral and straight tubes absorbed on glass substrates were subjected to 40 scans under a loading force of 29.93 nN. It was found that the spiral tube could be cut by the 40 scans across it. However, the straight tubes appear to be rigid and could not be cut by the 40 scans at the same conditions (Figure 3.6). Presumably, the strengthening of LCA tubes via the hydrogen bonding disrupts the balance between the chiral interaction and the elasticity. The chiral interaction is not strong enough to overcome the elastic energy of LCA tubes, leading to the spiral-to-straight shape transition at pH 7.4. The transition process is found to be reversible as the pH of solution was adjusted back to 12.0 with NaOH. In this case, the ionization of the COOH groups cleaves the hydrogen bonding between LCA molecules. The disassociation of hydrogen bonding (COOH-HOOC) and the electrostatic repulsion of the COO^- groups are expected to reduce the elastic modulus of LCA tubules, which is evident from their flexibility in solution at pH 12.0. In this case, the chiral interaction provides sufficient energy to compensate for the elastic penalty to

www.manaraa.com

coil the tubules into spirals. The decrease of elasticity of LCA tubes lead to the straight-to-spiral shape transition.

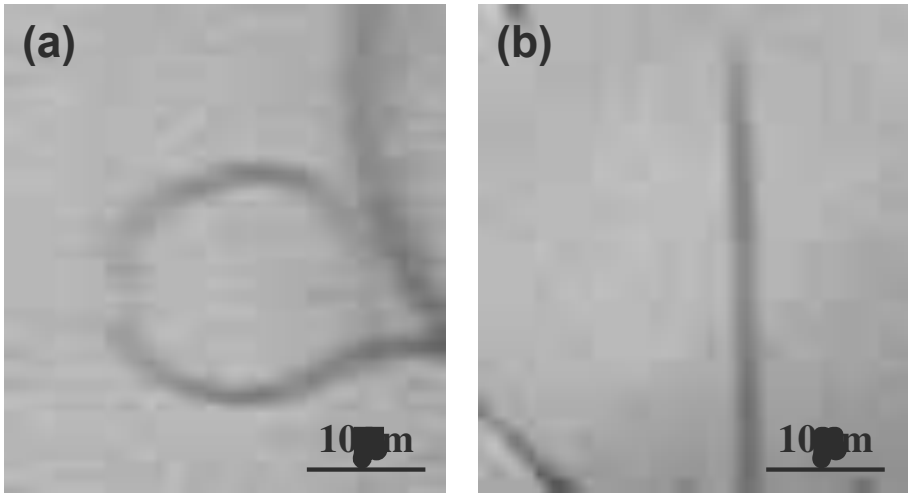

Figure 3.6 Optical microscopy images of coiled (a) and straight (b) tubes adsorbed on glass substrates after 40 scans under a loading force of 29.93 nN in aqueous solutions at pH 12.0 and pH 7.4, respectively. These images were taken with the optical microscope built into the AFM.

3.4 Conclusions

In summary, we report the formation of spiral tubes by the self-assembly of chiral LCA molecules in aqueous solutions at pH 12.0. The chirality presented in these supramolecular assemblies is of great interest from a biological point of view as well as for applications in materials science. Furthermore, the spiral LCA tubes transit into a straight shape as the pH of solution is reduced from 12.0 to 7.4. The spiral-to-straight shape transition is reversible when the

www.manaraa.com

pH is adjusted to 12.0. The pH-switchable tubes may act as a supramolecular spring in response to chemical and environmental stimuli.

3.5 References

1. Cook, T. A., *The Curves of Life.* (Dover, London, **1979**).
2. Gallow, J., *Helical Imperative: Paradigm of Form and Function.* (John Wiley & Sons, Ltd, **2002**).
3. Lehn, J. M., *Supramolecular Chemistry*. (Wiley-VCH, Weinheim, Germany **1995**).
4. Cornelissen, J. J. L. M.; Rowan, A. E.; R Nolte, J. M.; Sommerdijk, N, A. J. M., Chiral architectures from macromolecular building blocks. *Chem. Rev.*, **2001,** 101, 4039.
5. Fuhrhop, J. H.; helfrich, W., Fluid and solid fibers made of lipid molecular bilayers. *Chem. Rev*. **1993**, 93, 1565.
6. Hafkamp, R. J. H.; Feiters, M. C.; Nolte, R. J. M., Tunable supramolecular structures from a gluconamide containing imidazole. *Angew. Chem. Int. Ed*., **1994**, 33, 986.
7. Frankel, D. A.; O'Brien. D. F., Supramolecular assemblies of diacetylenic aldonamides. *J. Am. Chem. Soc*., **1994**, *116*, 10057.
8. John, G,; Mason, M.; Ajayan, P. M.; Dordick, J. S., Lipid-based nanotubes as functional architectures with embedded fluorescence and recognition capabilities. *J. Am. Chem. Soc*., **2004**, 126, 15012.
9. Nakashima, N.; Asakuma, S.; Kunitake, T., Optical microscopic study of helical superstructures of chiral bilayer-membranes. *J. Am. Chem. Soc*., **1985**, 107, 509.
10. Imae, T.; Takahashi, Y.; Muramatsu, H., Formation of fibrous molecular assemblies by amino-acid surfactants in water. *J. Am. Chem. Soc*., **1992**, 114, 3414.

www.manaraa.com

11. Shimizu, T.; Hato, M., Self-assembling properties of synthetic peptidic lipids. *Biochim. Biophys. Acta*, **1993**, 1147, 50.

12. Song, J.; Cheng, Q.; Kopta, S.; Stevens, R. C., Modulating artificial membrane morphology: pH-induced chromatic transition and nanostructural transformation of a bolaamphiphilic conjugated polymer from blue helical ribbons to red nanofibers. *J. Am. Chem. Soc*., **2001**, 123, 3205.

13. Zhan, C.; Gao, P.; Liu, M. M., Self-assembled helical spherical-nanotubes from an L-glutamic acid based bolaamphiphilic low molecular mass organogelator. *Chem. Commun*., **2005**, 462.

14. Zhang, S.; Holmes, T.; Lockshin, C.; Rich, A., Spontaneous assembly of self-complementary oligopeptide to form a stable macroscopic membrane. *Proc. Natl. Acad. Sci. USA.*, **1993**, 90, 3334.

15. Matsui, H.; Golongan, B., Crystalline glycylglycine bolaamphiphile tubules and their pH-sensitive structural transformation. *J. Phys. Chem. B*, **2000**, 104, 3383.

16. Fishwick, C. W. G.; Beevers, A. J.; Carrick, L. M.; Whitehous, C. D.; Aggeli, A.; Boden, N., Structures of helical beta-tapes and twisted ribbons: The role of side-chain interactions on twist and bend behavior. *Nano Lett.* **2003**, 3, 1475.

17. Li, L. S.; Jiang, H.; Messmore, B. W.; Bull, S. R., A torsional strain mechanism to tune pitch in supramolecular helices. Stupp. *Angew. Chem. Int. Ed.*, **2007**, 46, 5873.

18. Georger, J. H.; Singh, A.; Price, R. R.; Schnur, J. M.; Yager, P.; Schoen, P. E., Helical and tubular microstructures formed by polymerizable phosphatidylcholines. *J. Am. Chem. Soc.* **1987**, 109, 6169.

www.manaraa.com

19. Thomas, B. N.; Lindemann, C. M.; Clark, N. A., Left- and right-handed helical tubule intermediates from a pure chiral phospholipid. *Phys. Rev. E.*, **1999**,59, 3040.

20. Zhao, Y.; Mahajan, N.; Lu, R.; Fang, J. Y., Liquid-crystal imaging of molecular-tilt ordering in self-assembled lipid tubules. *Proc. Natl. Acad. Sci. USA.*, **2005,** 102, 7438,

21. Mahajan, N.; Zhao, Y.; Du, T. B.; Fang, J. Y., Nanoscale ripples in self-assembled lipid tubules. *Langmuir*, **2006**, *22*, 1973.

22. Fang, J. Y., Ordered arrays of self-assembled lipid tubules: fabrication and applications. *J. Mater. Chem.*, **2007**, 17, 3479.

23. Berthier, D.; Buffeteau, T.; Léger, J. M.; Oda, R.; Huc, I., From chiral counterions to twisted membranes. *J. Am. Chem. Soc*., **2002**, 124, 13486.

24. Brizard, A.; Aimé, C.; Labrot, T.; Huc, I.; Berthier, D.; Artzner, F.; Desbat, B.; Oda, R., Counterion, temperature, and time modulation of nanometric chiral ribbons from gemini-tartrate amphiphiles. *J. Am. Chem. Soc*., **2007**, 129, 3754.

25. Yanagawa, H.; Ogawa, Y.; Furuta, H.; Tsuno, K., Spontaneous formation of superhelical strands. *J. Am. Chem. Soc*., **1989**, 111, 4567.

26. Shimizu, T.; Iwaura, R.; Masuda, M.; Hanada, T.; Yase, k., Internucleobase-interaction-directed self-assembly of nanofibers from homo- and heteroditopic 1,omega-nucleobase bolaamphiphiles. *J. Am. Chem. Soc.,* **2001**, *123*, 5947.

27. Iwaura, R.; Shimizu, T., Reversible photochemical conversion of helicity in self-assembled nanofibers from a 1,omega-thymidylic acid appended bolaamphiphile. *Angew. Chem. Int. Ed.*, **2006**, 45, 4601.

www.manaraa.com

28. Chung, D. S.; Benedek, G. B.; Konikoff, F. M.; Donovan, J. M., Elastic free-energy of anisotropic helical ribbons as metastable intermediates in the crystallization of cholesterol, *Proc. Natl. Acad. Sci. USA*., **1993**, 90, 11341.

29. Zastavker, Y. V.; Asherie, N.; Lomakin, A.; Pande, J.; Donovan, J. M.; Schnur, J. M.; Benedek, G. B., Self-assembly of helical ribbons. *Proc. Natl. Acad. Sci. USA*. **1999**, 96, 7883.

30. E. Rogalska, M. Rogalski, T. Gulik- Krzywicki, A. Gulik, C. Chipot, Self-assembly of chlorophenols in water, *Proc. Natl. Acad. Sci. USA*. **1999**, *96*, 6577-6580.

31. Terech, P.; Talmon, Y., Aqueous suspensions of steroid nanotubules: Structural and rheological characterizations, *Langmuir* **2002**, 18, 7240.

32. Jean, B. ; Oss-Ronen, L. ; Terech, P.; Talmon, Y., Monodisperse bile-salt nanotubes in water: Kinetics of formation. *Adv. Mater*. **2005**, 17, 728.

33. Small, D. M., *In the Bile Acids: Chemistry, Physiology and Metabolism*; Nairm P. P., Kritchevski, D. Eds.; Plenum Press: New York, 1971; P249.

34. Oakenfull, D. G.; Fisher, L. R., Role of hydrogen-bonding in formation of bile-salt micelles. *J. Phys. Chem.* **1977**, 81, 1838.

35. Venkatesan, P.; Cheng, Y.; Kahne, D., Hydrogen-bonding in micelle formation. *J. Am. Chem. Soc.*, **1994**, 116, 6955.

36. Sachs, J., *Text-book of Botany, Morphological and Physiological.* (Clarendon Press, Oxford, **1875**).

37. Selinger, R. L. B.; Selinger, J. V.; Malanoski, A. P.; Schnur, J. M., Shape selection in chiral self-assembly. *Phys. Rev. Lett.* **2004**, 93, 158103.

www.manaraa.com

38. Leonard, M. R.; Bogle, M. A.; Carey, M. C.; Donovan, J. M., Spread monomolecular films of monohydroxy bile acids and their salts: Influence of hydroxyl position, bulk pH, and association with phosphatidylcholine. *Biochemistry* **2000,** 39, 16064.

39. Lin-Vien, D.; Colthup, N. B.; Fateley, W. G.; Grasselli, J. G., *The handbook of Infrared and Raman Characteristic Frequencies of Organic Molecules.* (Academic Press: New York, **1991**).

www.manaraa.com

CHPATER 4: FLUORESCENT COMPOSITE TUBES WITH PH-CONTROLLED SHAPES

4.1 Introduction

Self-assembled organic tubes with crystalline walls made of amphiphilic molecules have received considerable interest as controlled release vehicles for drug delivery,[1-4] encapsulates for functional molecules,[5-7] and nanoreactors for chemical reactions.[8-10] Unlike carbon nanotubes, which are hydrophobic by nature, self-assembled hollow organic tubes with hydrophilic surfaces provide biologically friend confinements for biotechnology applications.

It has been shown that self-assembled organic tubes have a moderate modulus (~ 1 GPa).[11] The soft organic tubes can be easily bent by shear flow and interface tension.[12] The self-assembled organic/inorganic composite tubes are particularly attractive because they can show dual physical properties. For example, the inorganic fraction might enhance mechanical strength and allow the tubes to sustain harsh environments, while the organic fraction provides biocompatible environments. Beyond that, the inorganic component such as inorganic nanoparticles may build additional functionalities such as specific optical, electric, and catalytic properties into organic tubes, which is of great interest for materials and biological applications.

Inorganic nanoparticles have attracted much interest during the past decades in both fundamental researches and technical applications because of their unique electrical and optical properties.[13] Progress has been made in depositing or patterning inorganic nanoparticles on the surface of pre-formed organic tubes.[12-20] However, it is still challenging in the synthesis of organic/inorganic composite tubes in which inorganic nanoparticles are embedded in the walls of

www.manaraa.com

self-assembled organic tubes. Although a number of amphiphilic molecules are capable of self-assembling into tubular structures and directing the deposition of inorganic nanoparticles on their surfaces, they often show no tendency of co-assembling with inorganic nanoparticles into tubular structures. An alterative approach for synthesizing organic/inorganic nanoparticles composite tubes is to use the self-assembly of transition-metal-complexed amphiphilic molecules.[21]

Lithocholic acid (LCA) is a secondary bile acid. It has been shown that LCA can self-assemble into tubular structures with different morphologies and shapes in aqueous solution by controlling the experimental condition under which self-assembly occurs. [22-24] In this chapter, we report the synthesis of fluorescent composite tubes in which the CdS nanoparticles are embedded in the membrane walls of self-assembled LCA tubes by the *in situ* assembly of LCA, $Cd(ClO_4)_2 \cdot 2H_2O$, and C_2H_5NS in aqueous solution. The structure and optical properties of the embedded CdS nanoparticles in the self-assembled LCA tubes are characterized. We find that the embedded CdS nanoparticles make the LCA tubes fluorescent for months. The shape of fluorescent composite tubes can be changed by altering the pH of aqueous solution. The fluorescent LCA tubes with embedded CdS nanoparticles are promise in materials and biological applications. In addition, the membrane walls can also act as a shield to protect the embedded CdS nanoparticles from environments. The fluorescent nature of the composite tubes allows us to visualize their location in biological systems.

Here we describe the synthesis of fluorescent composite tubes in which cadmium sulfide (CdS) nanoparticles are embedded in lithocholic acid (LCA) membrane walls. The LCA/CdS composite tubes are characterized by transmission electron microscopy, Fourier transform infrared

www.manaraa.com

(FT-IR) spectra, ultraviolet-visible (UV-vis) absorption spectroscopy, and confocal fluorescence microscopy. The CdS nanoparticles embedded in LCA membrane walls make the tubes fluorescent for months. The fluorescent composite tubes show pH-dependent shapes. At pH 9.5, they show a straight shape, while at pH 13.0 they coil into a left-handed helix.

4.2 Experimental sections

4.2.1 Chemicals and materials

Cadmium perchlorate hydrate ($Cd(ClO_4)_2 \cdot 2H_2O$), thioacetamide (C_2H_5NS), sodium hydroxide (NaOH), and lithocholic acid (LCA) were purchased from Aldrich and used without further purification. Distilled, deionized water used in our experiments was purified with Easypure II system (18 MΩ cm, pH 5.7). Microscope cover glass slides were purchased from Fisher Scientific. Carbon-coated TEM grids were from Allied High Tech Products, Inc.

4.2.2 Synthesis of LCA/CdS composite tubes

The synthesis of LCA/CdS composite tubes in aqueous solution was conducted at room temperature. First, 30 mg of LCA was added to 10 mL of water. The pH of LCA solution was adjusted by adding NaOH. The LCA solution was vortexed until the LCA was completely dissolved. Second, 0.5 mL stock solution of $Cd(ClO_4)_2 \cdot 2H_2O$ with a concentration of 2 mM was added into 10 mL of the freshly prepared LCA solution, followed by adding 0.5 mL C_2H_5NS solution with a concentration of 2 mM. A transition from a translucent into a yellowish solution occurred after 1 hour.

www.manaraa.com

4.2.3 Characterization of LCA/CdS composite tubes

Optical microscopy observation of LCA/CdS composite tubes was carried out an Olympus BX40 microscope with a digital camera (Olympus C2020 Zoom). Transmission electron microscopy (TEM) was performed with a JEOL JEM100SX-EM microscope operating at an acceleration voltage of 100 kV for the morphology investigation of LCA/CdS composite tubes and a FEI Technai F30 TEM at an acceleration voltage of 300 kV for the structure analysis of the embedded CdS nanoparticles, respectively. Ultraviolet-visible (UV-*vis*) absorption spectra of LCA/CdS composite tubes were obtained with a Cary 300 spectrophotometer. Fourier transform infrared (FT-IR) spectra of pure LCA and LCA/CdS composite tubes were recorded with a PerkinElmer 100 spectrometer equipped with a DTGS KBr detector. Fluorescence images and spectra of individual LCA/CdS composite tubes were obtained with a confocal fluorescence microscope. The detail of the confocal fluorescence microscope has been described elsewhere.[25] Briefly, the excitation source at 488 nm was derived from the laser lines of an Ar^+ laser (Spectra-Physics, Mt. View, CA), which was brought to a focus in individual composite tube by a microscope objective. The emission was collected with the same objective and was separated from the excitation light by a dichroic mirror. A single interference filter was used to allow only the fluorescence pass through and reach the detector. Confocal fluorescence images were acquired by moving the coverslip mounted on a high-resolution piezo-controlled nanopositioning and scanning translation state. A power of ~ 60 nW was used in the imaging experiments.

www.manaraa.com

4.3 Results and discussion

4.3.1 Structure of LCA/CdS tubes

LCA has a nearly planar hydrophobic steroid nucleus, with four hydrogen atoms and one hydroxyl group directed toward the concave side, and the convex side with three methyl groups. The carboxylic acid group is linked to the steroid ring through a short alkyl chain (Figure 2.1a). The solubility of LCA in aqueous solution can be dramatically increased if the pH of solution is raised to alkaline values. The self-assembly of LCA-CdS composite tubes were carried out in a mixed solution, which were prepared by adding 0.5 mL solution containing 2mM $Cd(ClO_4)_2 \cdot 2H_2O$ into 10 mL of freshly prepared LCA solution with pH of 9.5, followed by adding 0.5 mL solution containing 2 mM C_2H_5NS after 1 min. After aging in a sealed glass vial for one hour at room temperature, the solution tuned yellow.

Our previous studies have showed that the self-assembly of pure LCA tubes in aqueous solution is a slow process.[24] Here we find that the presence of $Cd(ClO_4)_2 \cdot 2H_2O$ and C_2H_5NS in aqueous solution does not effect the self-assembly capability of LCA. Interestingly, the methods stated above allow us to form composite tubes in which the CdS nanoparticles are embedded in the membrane walls of LCA. The pK_a value of the LCA is 7.0 ~ 8.4 in crystalline monolayers.[26] Therefore, we expect that the COOH group of LCA molecules in aqueous solution is protonated at the pH 9.5. The protonated LCA molecules provide the negatively charged COO^- active sites to coordinate with Cd^{2+} ions. Although we have not fully understood the formation mechanism of LCA-CdS composite tubes, it is likely that the coordinated Cd^{2+} *in situ* reacts with S^{2-} to form CdS

www.manaraa.com

seeds during the self-assembly of LCA-Cd molecules, and eventually grow into CdS nanoparticles inside the membrane walls of LCA tubes.

Figure 4.1a show an optical microscopy image of composite LCA/CdS tubes. We find that the composite tubes have a straight shape with a length up to 60 μm. The diameter of the composite

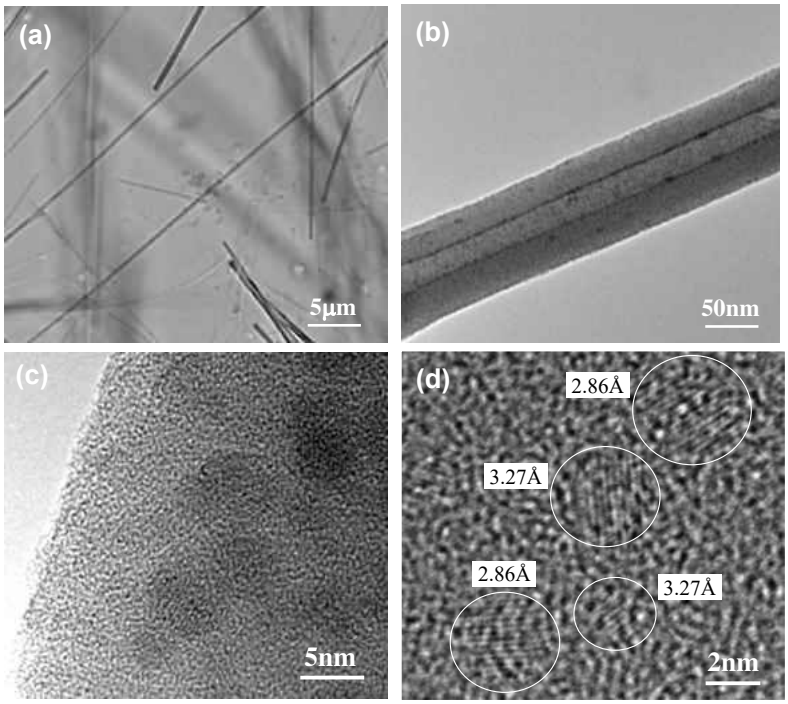

Figure 4.1 (a) Optical microscopy image of composite LCA/CdS tubes in aqueous solution at pH 13.0. (b) Low resolution TEM image of a LCA/CdS tubes dried on a carbon-coated grid. (c-d) high resolution TEM images of individual CdS nanoparticles embedded in LCA membrane walls.

tubes is in the range from 170 to 250 nm. Figure 1b is a low-resolution TEM image of a composite LCA/CdS composite tube, which shows that the hollow composite tube has a uniform inner diameter of ~ 50 nm and a wall thickness of ~ 60 nm. The CdS nanoparticles appear as dark dots

www.manaraa.com

with a diameter of 4~6 nm in the TEM image. The TEM image taken at the boundary of a composite tube shows that the CdS nanoparticles are embedded inside the tube wall, rather than deposited at the tube surface (Figure 1c). The structure of the CdS nanoparticles embedded in the tube walls was further characterized with a high-resolution TEM. We find that that the CdS nanoparticles are loosely embedded in the tube walls without aggregation and show lattice fringes with an interplanar spacing of 3.27 and 2.86 Å (Figure 1d), which correspond to the (111) and (200) planes of the cubic (zinc blende) CdS structure.[27-28] This indicates the formation of high-quality cubic CdS nanocrystals.

Figure 4.2a shows an absorption spectrum of LCA-CdS composite tubes, which was taken in solution. The CdS nanoparticles embedded in the tube walls exhibit an absorption shoulder around 480 nm, which relate to the excitation state of CdS nanoparticles. The absorption edge is close to that of the bulk CdS (510 nm) since the size of the embedded CdS nanoparticles is close to that of an exciton of bulk CdS whose absorption edge is near 510 nm.[29] It has shown that there is no quantum confinement for the CdS nanoparticles whose size is larger than 5 nm.[30] Figure 2b shows the FT-IR spectra of pure LCA tubes and LCA-CdS composite tubes formed at pH 9.5. The absorption bands at 2857 and 2925 cm^{-1}, which are observed for both LCA tubes and LCA-CdS composite tubes, can be straightforwardly assigned to the stretching vibration of the CH_2 in the short acyl chain of LCA molecules. In the carbonyl stretching region, we observe the signal of both the COO^- group at 1546 cm^{-1} and the COOH group at 1706 cm^{-1} for pure LCA tubes, which indicates the existence of deprotonated LCA and protonated LCA molecules. It has been reported that the non-associated COOH groups show an absorption peak at about 1750 cm^{-1}, while the association of COOH groups through hydrogen bonding shows an absorption peak at about 1700

www.manaraa.com

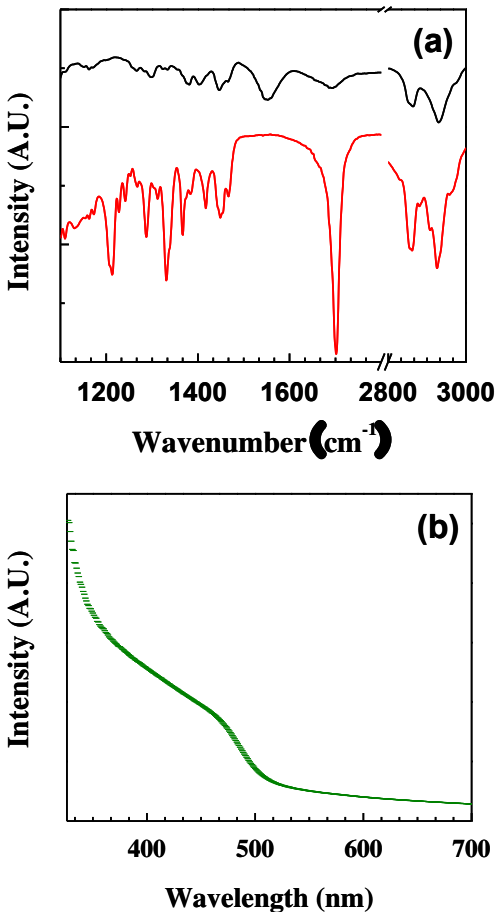

Figure 4.2 (a) FT-IR spectra of pure LCA tubes and composite LCA/CdS tubes dried on an ATR crystal. (b) UV-vis spectrum of composite LCA/CdS tubes in aqueous solution. Both FT-IR and UV-vis spectra were taken at room temperature.

cm^{-1}.[31] Therefore, we conclude that the COOH of a protonated LCA molecule associate itself in hydrogen bonding with the OH group or the COOH of another LCA molecule. It is noticeable that the absorption band of the COO^- group disappears in the LCA/CdS composite tubes formed at pH 9.5. Instead we observe an intensified absorption band of the COOH group. The chemical reaction toward the formation CdS nanoparticles can be summarized as:

$$Cd^{2+} + CH_3C(S)NH_2 + H_2O \rightarrow CdS + CH_3C(O)NH_2 + 2\ H^+$$

www.manaraa.com

Therefore, it is likely that the competitive binding of H^+ produced by the chemical reaction to the COO^- groups leads to the disappearance of the COO^- group and the intensified absorption band of the COOH group.

4.3.2 Optical properties of LCA/CdS compsite tubes

The optical properties of individual LCA/CdS composite tubes were further characterized

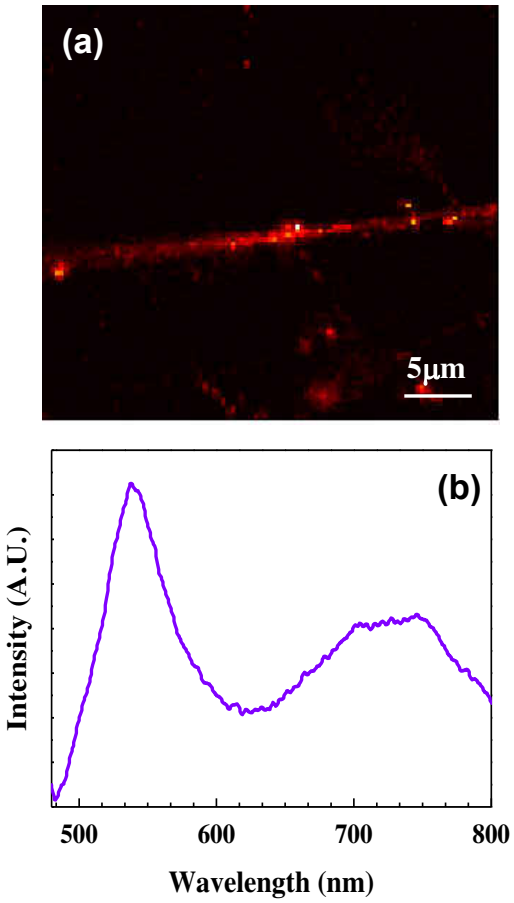

Figure 4.3 (a) Fluorescence confocal image of a composite LCA/CdS tubes in aqueous solution at pH 9.5. (b) Fluorescence spectrum taken from a simple point at the composite LCA/CdS tube shown in (a).

www.manaraa.com

by a confocal fluorescence microscope with an excitation at 488 nm. As can be seen from Figure 4.3a, the composite tubes are lighted up by the embedded CdS nanoparticles. The observed fluorescence originates from the electronic transition of the CdS nanoparticles embedded in the tube wall. The fluorescence spectrum from a single spot on the LCA/CdS composite tube under the excitation at 488 nm shows a relatively sharp emission band at ~ 530 nm and a broad red emission band with the center at ~ 750 nm (Figure 4.3b). The sharp band at 530 nm represents the intrinsic emission of the embedded CdS nanoparticles. The relatively sharpness of the emission band indicates a narrow size distribution of the embedded CdS nanoparticles, which agrees with our TEM measurements. The broad red emission band with a center of 750 nm is attributed to the recombination of charged carriers trapped in the surface state (trapped state), which is a result of the defect at the surface of the embedded CdS nanoparticles.[32]

The LCA/CdS composite tubes become unstable and break into small spherical vesicles when the pH of aqueous solution is increased from 9.5 to 13.0 by adding NaOH. These newly formed vesicles show strong fluorescence as well (Figure 4.4a), suggesting that they contains CdS nanoparticles. The LCA/CdS composite vesicles collapse into flat patches after dried on carbon-coated grids (Figure 4.4b). As can be seen, the CdS nanoparticles with a diameter of 5-6 nm (dark dots) are uniformly distributed within the plates without any central aggregation. Therefore, we infer that the CdS nanoparticles were embedded in the shell of the spherical LCA vesicles rather than encapsulated in their aqueous interior. The corresponding energy dispersive X-ray (EDX) spectrum of the Figure 4b confirms the presence of Cd and S components (Figure 4.4c). The CdS nanoparticles embedded in the LCA patches also show the characteristic lattice fringe of the (111) plane of cubic CdS nanocrystals with an interplanar spacing of 3.2 nm (Figure

www.manaraa.com

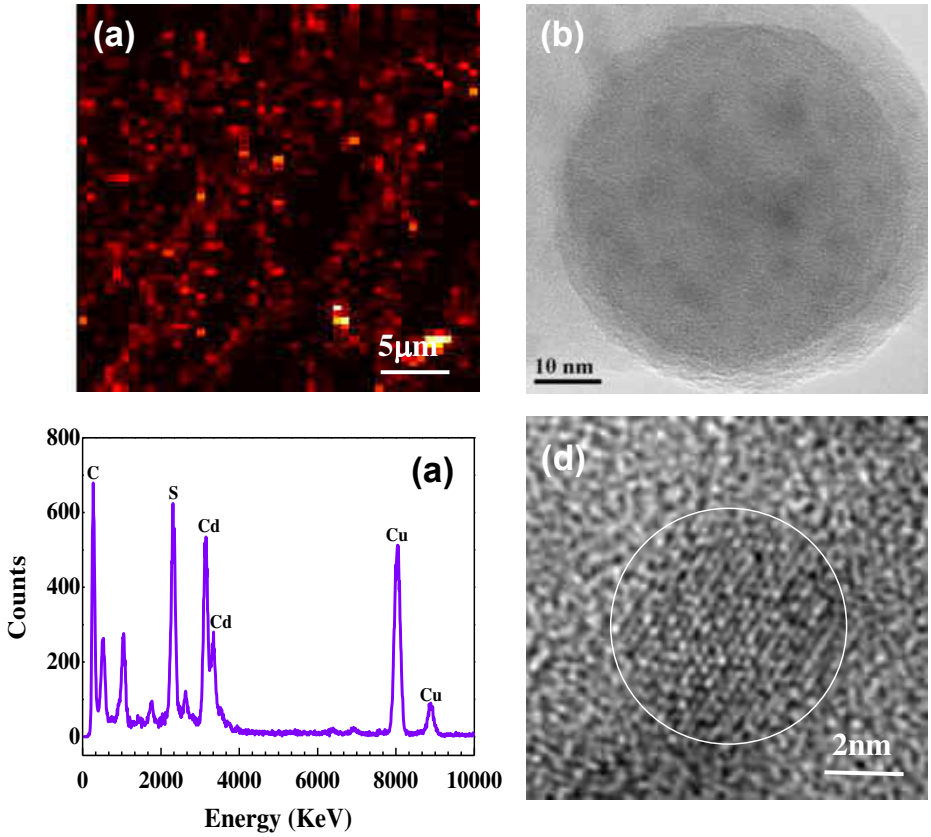

Figure 4.4 (a) Fluorescence confocal image of a composite LCA/CdS vesicle in aqueous solution at pH 13.0. (b) Low-resolution TEM image of a collapsed LCA/CdS vesicle on a carbon-coated grid. (c) EDX spectrum of the collapsed LCA/CdS vesicle shown in (b). (d) high-resolution TEM images of individual CdS nanoparticles embedded in the collapsed LCA/CdS vesicle shown in (b).

4.4d). The size of the CdS nanoparticles embedded in the shell of LCA vesicles agrees with that in the wall of LCA tubes.

www.manaraa.com

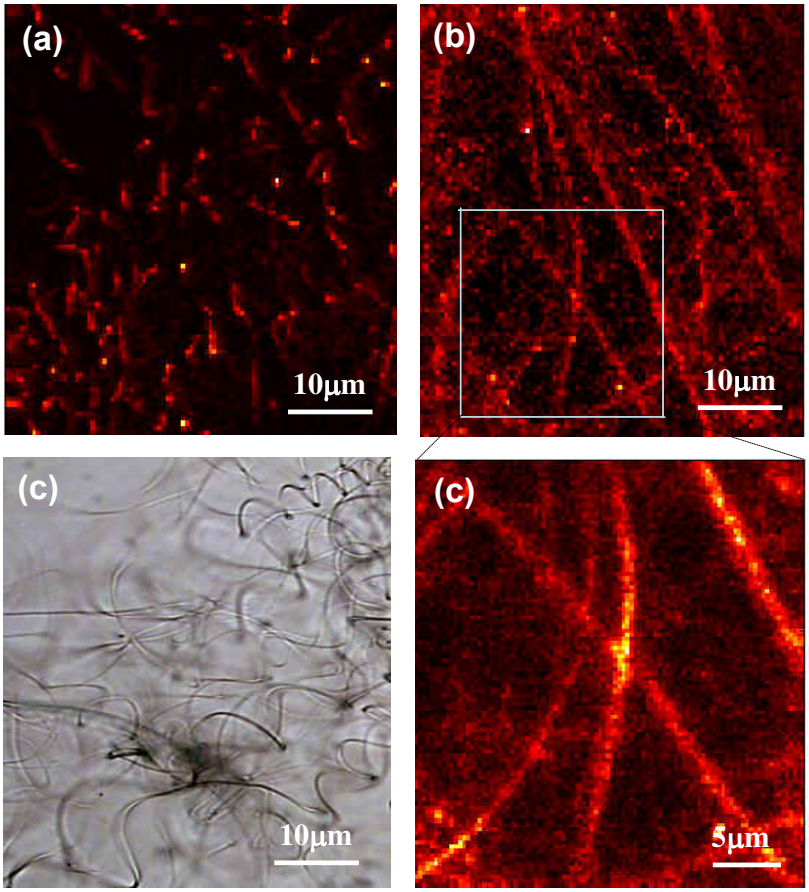

Figure 4.5 (a) Fluorescence confocal image of linearly aggregated composite LCA/CdS vesicles in aqueous solution at pH 13.0. (b) Fluorescence confocal image of composite LCA/CdS tubes in aqueous solution at pH 13.0. (c) Enlarged Fluorescence confocal image of the selected are in (a). (d) Optical microscopy image of helical composite LCA/CdS tubes in aqueous solution at pH 13.0.

4.3.3 Conformation changes of LCA/CdS composite

Interestingly, the composite LCA/CdS vesicles linearly aggregate over time (Figure 4.5a). The fusion of these linearly aggregated vesicles leads to the formation of flexible fluorescent tubes, which show a curved shape (Figure 4.5b). The homogeneity of the fluorescence intensity

www.manaraa.com

along the tubes suggests that the CdS nanoparticles are rather uniformly embedded in the tube walls (Figure 4.5c). The self-assembled mechanism of LCA tubes differs from that of other bile acid tubes in which the helical ribbons are a precursor.[33-35] We find that the composite tubes continuously grow until all vesicles are consumed. Eventually, the reassembled composite tubes at pH 13.0 tend to coil into helical shape (Figure 4.5d). The handedness of helical composite tubes is difficult to be determined by an optical microscope since their apparent handedness changes during a through-focus imaging. We find that the 3D spiral tubes gradually deposit on the glass substrate and contract into 2D spirals with water evaporation (Figure 3.2). In this case, the handedness of spiral tubes can be unambiguously determined by positioning the microscope objective focal plane at the substrate. All spiral tubes are found to be left-handed. The microscopic handedness of spiral tubes should be tied to the intrinsic chirality of the steroid nucleus of the LCA. The microscopic handedness of helical composite tubes should be tied to the intrinsic chirality of the steroid nucleus of LCA. In other words, the chirality of individual LCA molecules is expressed in their supramolecular composites. The change in the apparent diameter of the spiral tubes is a result of the defocus under optical microscope.

It is known that the self-assembly of molecules is driven by intermolecular interactions.[36] The shape and stability of self-assembled LCA/CdS tubes are a result of the balance of intermolecular interactions. As the pH of solution is increased from 9.5 to 13.0, the LCA molecules in the straight composite tubes are protonated. The ionization of the COOH groups causes electrostatic repulsion between LCA molecules, which disrupts the origin balance of intermolecular interactions, leading to the breaking of the straight composite tubes. The reassembly of coiled composite tubes at pH 13.0 is a result of the new balance of intermolecular

www.manaraa.com

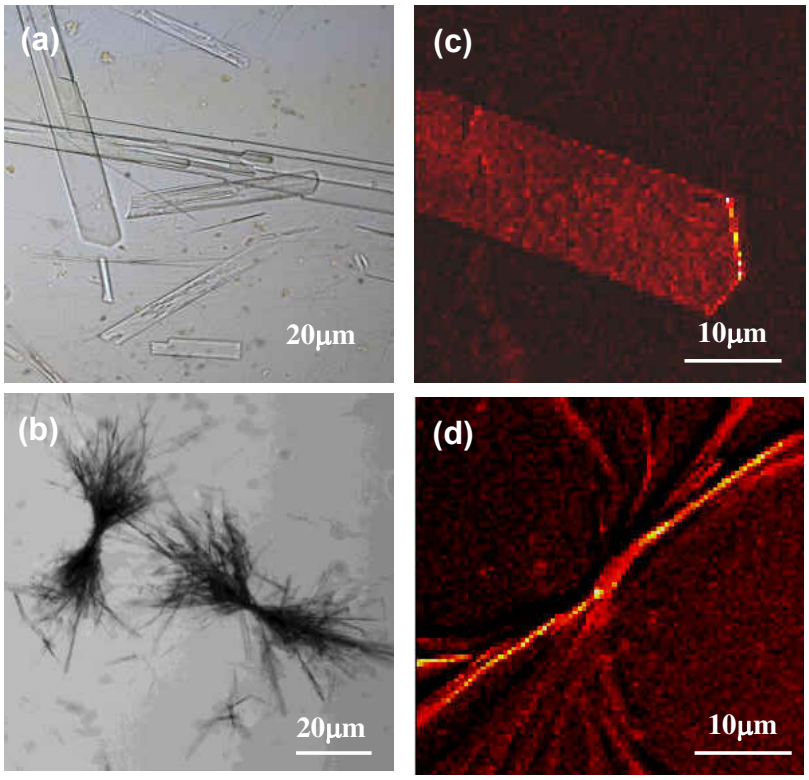

Figure 4.6 Optical microscopy (a) and fluorescence confocal (b) images of composite LCA/CdS plates in aqueous solution at pH 7.0. Optical microscopy (c) and fluorescence confocal (d) images of composite sheaves in aqueous solution at pH 5.0.

interactions. Mesoscale simulations have shown that the shape of one-dimensional self-assembled supramolecular structures of chiral molecules is determined by the balance between their elasticity and chirality.[37] The shape transition of one-dimensional chiral aggregates can be achieved by varying their elastic modulus. In our case, the chiral interaction of the steroid nucleuses is believed to the main driving force for the coiling of LCA tubes. At pH 9.5, the hydrogen bonding between of LCA molecules are expected to reduce their mobility and strengthen the LCA/CdS composite

www.manaraa.com

tubes. While at pH 13.0, the electrostatic repulsion between LCA molecules weakens the elastic moodulus of LCA/CdS composite tubes. The chiral interaction of LCA molecules provides sufficient energy to compensate the elastic penalty to helically coil the composite tubes.

If the self-assembly was carried out at lower pH values, the different morphologies of LCA/CdS supramolecular assemblies are formed. We observed the formation of elongated plates at pH 8.5 (Figure 4.6a) and sheaves at pH 7.4 (Figure 4.6b), respectively. The observed fluorescence indicates that CdS nanoparticles embedded in the LCA plates and sheaves. The composite LCA/CdS plates are a few of micrometers in width and 20-50 micrometers in length. Some of the plates show terraced structures, suggesting that they are multilayer structures. The composite LCA/CdS sheaves consist of a number of rods which are tied in their middle with two tails fanning out. Both fantails of the sheave are almost identical.

4.4 Conclusions

We have synthesized fluorescent composite tubes in which CdS nanoparticles are embedded in the walls of self-assembled LCA tubes. The structure and optical properties of composite LCA/CdS tubes are characterized by TEM, UV-vis spectroscopy, FT-IR spectroscopy, and confocal fluorescence microscopy. Our experimental data clearly show that the fluorescence of composite tubes comes from the embedded CdS nanoparticles with the cubic (zinc blende) crystal structure. As the fluorescence of CdS nanocrystals is bright, easily distinguishable, and resistant to photobleaching, long-term fluorescence microscopy observation of LCA tubes becomes feasible. The shape of LCA/CdS composite tubes depends on the pH of solution under which the self-assembly takes place. We find that the LCA/CdS tubes show a straight shape at

www.manaraa.com

pH 9.5 and a helically coiled shape at pH 13.0. The fluorescent composite tubes with pH-switchable shapes are promise in materials and biological applications.

4.5 References

1. Schnur, J. M.; Price, R.; Rudolph, A. S. Biologically engineered microstructures – controlled- release applications, J. Control. Release. **1994**, 28, 3.

2. Meilander, N. J.; Pasumarthy, M. K.; Kowalczyk, T. H.; Cooper, M. J. Bellamkonda, R. V. Sustained release of plasmid DNA using lipid microtubules and agarose hydrogel, J. Control. Release. **2003**, 88, 321.

3. Guo, L.; P.Chowdhury, P.; Fang, J. Y.; Gai, F. Heterogeneous and anomalous diffusion inside lipid tubules, J. Phys. Chem. B **2007**, 111, 14244.

4. Kameta, N.; Minamikawa, H.; Masuda, M.; Mizuno, G.; Shimizu, T. Controllable biomolecule release from self-assembled organic nanotubes with asymmetric surfaces: pH and temperature dependence, Soft Matt. **2008**, 4, 1681.

5. N. Kameta, M. Masuda, H. Minamikawa, N. V. Goutev, J. A. Rim. J. H. Jung, and T. Shimizu, Selective construction of supramolecular nanotube hosts with cationic inner surfaces, Adv. Mater. **2005**, 17, 2732.

6. Yu, L. T.; Banerjee, I, A.; Gao, X. Y.; Nuraje, N.; Matsui, H. Fabrication and application of enzyme-incorporated peptide nanotubes, Bioconjugate Chem. **2005,** 16, 1484-1487.

7. Zhao, Y.; Mahajan, N.; Fang, J. Y. Self-assembled cylindrical lipid tubules with a birefringent core, Small. **2006**, 2, 364.

www.manaraa.com

8. Kameta, N.; Masuda, M.; Minamikawa, H.; Mishima, Y.; Yamashita, I.; Shimizu, T. Functionalizable organic nanochannels based on lipid nanotubes: Encapsulation and nanofluidic behavior of biomacromolecules, Chem. Mater. **2007**, 19, 3553.

9. Karlsson, A.; Sott, K.; Markström, M.; Davidson, M.; Komkoli, Z.; Orwar. O. Controlled initiation of enzymatic reactions in micrometer-sized biomimetic compartments, J. Phys. Chem. B. **2005**, 109, 1609.

10. Sott, K.; Lobovkina, T.; Lizana, L.; Tokarz, M.; Bauer, B.; Konkoli, Z.; Orwar, Controlling enzymatic reactions by geometry in a biomimetic nanoscale network, O. Nano Lett. **2006**, 6, 209.

11. Zhao, Y.; Tamhane, K.; Zhang, X.; An, L.; Fang, J. Y. Radial elasticity of self-assembled lipid tubules, ACS Nano **2008**, 2, 1466-1472.; Y. Zhao, Y.; An, L.; Fang, J. Y. Buckling instability of lipid tubules with multibilayer walls under local radial indentation, Phys. Rev. E **2009**. 80, 021911.

12. Mahajan, N.; Fang, J. Y. Two-dimensional ordered arrays of aligned lipid tubules on substrates with microfluidic networks, Langmuir **2005**, 21, 3153.; Zhao, Y.; An, L.; Fang, J. Y. Buckling of lipid tubules in shrinking liquid droplets, Nano Lett. **2007**, 7, 1360-1363.; Zhao, Y.; Fang, J. Y. Zigzag lipid tubules, J. Phys. Chem. B **2008**, 112, 10964.

13. Alivisatos, A. P. Semiconductor clusters, nanocrystals, and quantum dots, Science **1996**, 271, 933.

14. Baral S.; Schoen, P. Silica-deposited phospholipid tubules as a precursor to hollow submicron-diameter silica cylinders, Chem. Mater. **1993**, 5, 145.

www.manaraa.com

15. Lvov, Y. M.; Price, R. R.; Selinger, J. V.; Singh, A.; Spector, M. S.; Schnur, J. M. Imaging nanoscale patterns on biologically derived microstructures, Langmuir **2000,** 16, 5932.

16. Patil, A. J.; Muthusamy, E.; Seddon, A. M.; Mann, S. Higher-order synthesis of organoclay pipes using self-assembled lipid templates, Adv. Mater. **2003**, 15, 1816.

17. Zhou, Y.; Ji, Q.; Masuda, M.; Kamiya, S.; Shimizu, T. Helical arrays of CdS nanoparticles tracing on a functionalized chiral template of glycolipid nanotubes, Chem. Mater. **2006**, 18, 403.

18. Jung, J. H.; Rim. J. A.; Lee, S. J.; Lee, S. S. Spatial organization and patterning of palladium nanoparticles on a self-assembled helical ribbon lipid, ChemComm. **2005**, 468.

19. Takahashi, R.; Ishiatari, T. Preparation of helical gold nanowires on surfactant tubules, ChemComm. **2004**, 1406.

20. Terech, P.; Sangeetha, N. M.; Bhat, S.; Allegraud, J-J.; Buhler, E. Ammonium lithocholate nanotubes: stability and copper metallization, Soft Matter **2006**, 2, 517.

21. Zhou, Y.; Kogiso, M.; He, C.; Shimizu, Y.; Koshizaki, N.; Shimizu, T. Fluorescent nanotubes consisting of CdS-embedded bilayer membranes of a peptide lipid, Adv. Meter. **2007**, 19, 1055-1058. Zhou, Y.; Kogiso, M.; Asakawa, M.; Dong, S.; Kiyama, R.; Shimizu, T. Antimicrobial Nanotubes Consisting of Ag-Embedded Peptidic Lipid-Bilayer Membranes as Delivery Vehicles, Adv. Meter. **2009**, 21, 1741.

22. Terech, P.; Talmon, Y. Aqueous suspensions of steroid nanotubules: Structural and rheological characterizations, Langmuir **2002**, 18, 7240-7244.; Jean, B.; Oss-Ronen, L.; Terech, P.; Talmon. Y. Monodisperse bile-salt nanotubes in water: Kinetics of formation, Adv. Mater. **2005**, 17, 728.

www.manaraa.com

23. Pal, A.; Basit, H.; Sen, S.; Aswal, V. K.; Bhattacharya, A. Structure and properties of two component hydrogels comprising lithocholic acid and organic amines, J. Mater. Chem. **2009**, 19, 4325.

24. Zhang, X. J.; Zou, J. H.; Tamhane, K.; Kobzeff, F. F.; Fang, J.; J.; Self-Assembly of pH-Switchable Spiral Tubes: Supramolecular Chemical Springs, Small **2009**, 5, 366.

25. Tenery, D.; Worden, J. G.; Hu, Z. J.; Gesquiere, A. J. Single particle spectroscopy on composite MEH-PPV/PCBM nanoparticles, J. Lumines. **2009**, 129, 423.

26. Leonard, M. R.; Bogle, M. A.; Carey, M. C.; Donovan, J. M. Spread monomolecular films of monohydroxy bile acids and their salts: Influence of hydroxyl position, bulk pH, and association with phosphatidylcholine, Biochemistry **2000,** 39, 16064.

27. Diaz, D.; Rivera, M.; Ni, T.; Rodriguez, J. C.; Castillo-Blum, S. E.; Nagesha, D.; Robles, J.; Alvarez-Fregoso, O. J.; Kotov, N. A. Conformation of ethylhexanoate stabilizer on the surface of CdS nanoparticles, J. Phys. Chem. B **1999**, 103, 9854.

28. Torimoto, T.; Yamashita, M.; Kuwabata, S.; Sakata, T.; Mori, H.; Yoneyama, H. Fabrication of CdS nanoparticle chains along DNA double strands, J. Phys. Chem. B **1999,** 103, 8799.

A. Henglein, A. Small-particle research – physicochemical properties of extremely samll colooidal metal and semiconductor paticles, Chem. Rev. **1989**, 89, 1861.

29. Spanhel, L.; Haase, M.; Weller, H.; Henglein. A. Photochemistry of colloidal semiconductors .20. surface modification and stability of strong luminescing CDS particles, J. Am. Chem. Soc. **1987**, 109**,** 5649.

www.manaraa.com

30. Lichkus, A. M.; Painter, P. C.; Coleman, M. M. Hydrogen-bonding in polymer blends. 5. blends involving polymers containing methacrylic-acid and oxazoline groups, Macromolecules **1998**, 21, 2636.

31. Gao T.; Wang, T. Catalyst-assisted vapor-liquid-solid growth of single-crystal CdS nanobelts and their luminescence properties, J. Phys, Chem. B **2004**, 108, 20045.

32. Chung, D. S.; Benedek, G. B.; Konikoff, F. M.; Donovan, J. M.; Elastic free-energy of anisotropic helical ribbons as metastable intermediates in the crystallization of cholesterol, Proc. Natl. Acad. Sci. USA. **1993**, 90, 11341.

33. Zastavker, Y. V.; Asherie, N.; Lomakin, A.; Pande, J.; Donovan, J. M.; Schnur, J. M.; Benedek, G. B. Self-assembly of helical ribbons, Proc. Natl. Acad. Sci. USA. **1999**, 96, 7883.

34. Rogalska, E.; Rogalski, M.; Gulik- Krzywicki, T.; Gulik, A.; Chipot, C. Self-assembly of chlorophenols in water, Proc. Natl. Acad. Sci. USA. **1999**, 96, 6577.

35. Whitesides, G. M.; Grzybowski, B. Self-assembly at all scales, Science **2002**, 295, 2418.

36. Selinger, R. L. B.; Selinger, J. V.; Malanoski, A. P.; Schnur, J. M. Shape selection in chiral self-assembly, Phys. Rev. Lett. **2004**, 93, 158103.

www.manaraa.com